Electronic Supplementary Material (ESI) for RSC Advances.

Supporting Information

Thioester-anchored organosilatranes: Synthetic investigations and applications in Cu^{2+} ion binding and fabrication of hybrid silica nanoparticles

Gurjaspreet Singh*, Sunita Rani, Amandeep Saroa, Shally Girdhar, Jandeep Singh, Aanchal Arora, Darpandeep Aulakh, Mario Wriedt*

Table of contents

Optimization of reaction conditions

To start with, the thioester formation from free carboxylic acid **3a** and MPS was examined. As expected, the reaction did not proceed at all (Table 1, entry 1); indicating that direct thioesterification is not possible under simple azeotropic reflux conditions. The catalytic activity of conc. H_2SO_4 was also tested for the reaction and only 30% product yield was achieved after 8 h (entry 2). In literature, there are different ways for activating carboxyl component of carboxylic acids in the form of acyl halides, acyl azides, acylimidazoles, anhydrides etc [1]. The commonly used method for the synthesis of thioesters involves the conversion of carboxylic acids into more reactive acyl chlorides, their isolation, and then reaction with thiols. Although with this method, the reaction could be accomplished in a short time period (5 h), but the moisture sensitivity of acyl chlorides, handling of thionyl chloride and formation of toxic HCl gas were the main disadvantages. Besides this, in the coupling of the acid chloride with MPS, an additional base was required to soak up the by-product HCl (Scheme 1).

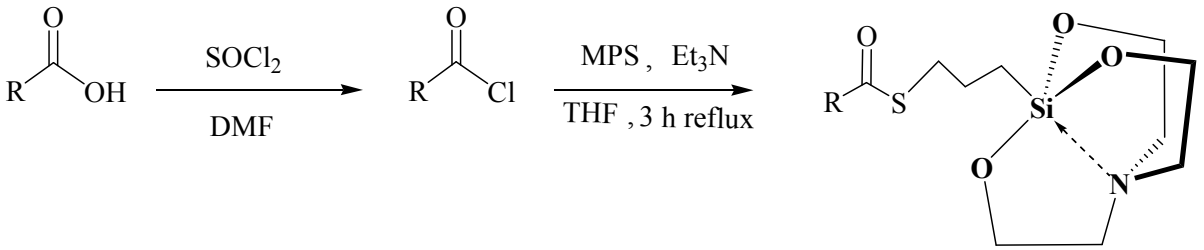

Scheme 1: Synthesis of ThE-OS derivatives using acid chlorides

These unavoidable limitations associated with this method enforced us to use some other coupling reagents. As CDI is fairly cheap, readily available and capable of generating clean reactions with innocuous by-products, we have therefore opted for the CDI mediated coupling of acids with MPS. Initially with carboxylic acid:CDI in 1:1 ratio, only 50% yield was obtained. The reaction was further attempted with acid and CDI in different ratios (Table 1, entries 5-7). Using 1:1.2 ratio of acid and CDI respectively, yield of the product improved considerably from 50 to 76%. No further improvement was observed by changing the ratios (entries 6 and 7). The solvent screening investigations revealed that THF is a better choice amongst all tried solvents (entries 8-10). Altogether, we can say that the CDI mediated coupling of heterocyclic carboxylic acids with MPS serves as an attractive route to integrate aromatic thioesters with silatranyl unit.

1. S. Iimura, K. Manabe and S. Kobayashi, *Chem. Commun.*, **2002**, 94–95.

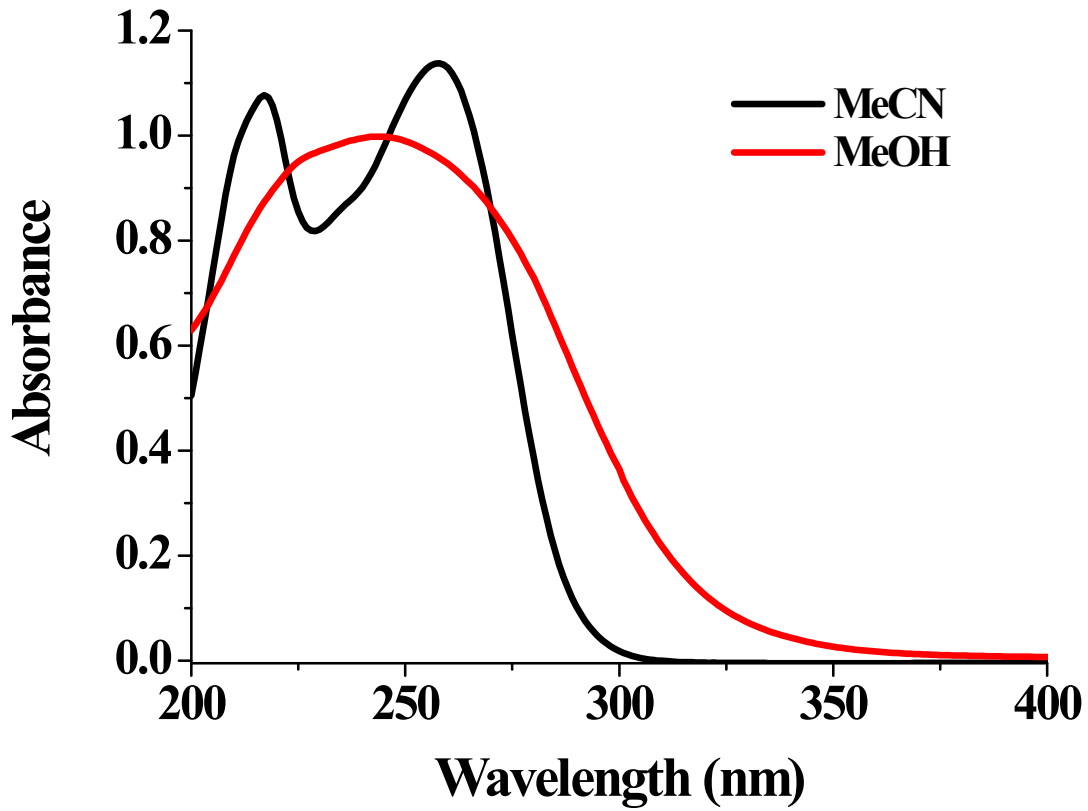

Fig. S1 UV-Vis plot of **3a** (0.1 mM) in acetonitrile and methanol

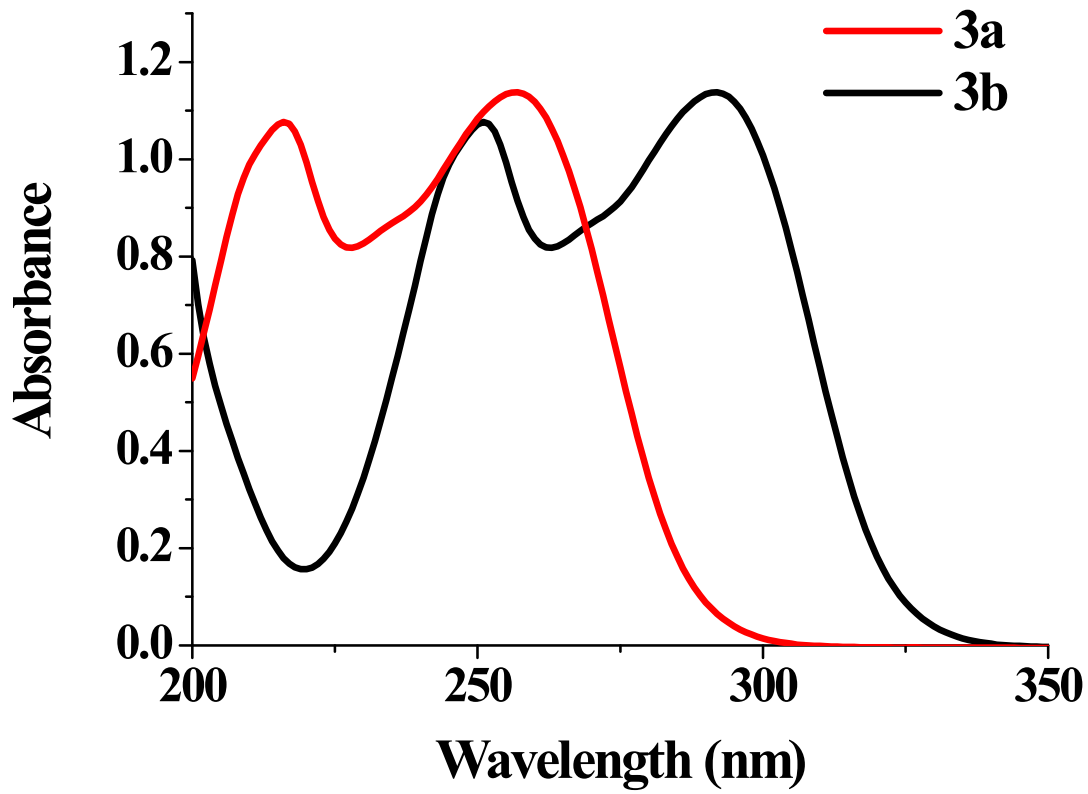

Fig. S2 UV-Vis plot of **3a** and **3b** at 0.1 mM concentration in acetonitrile

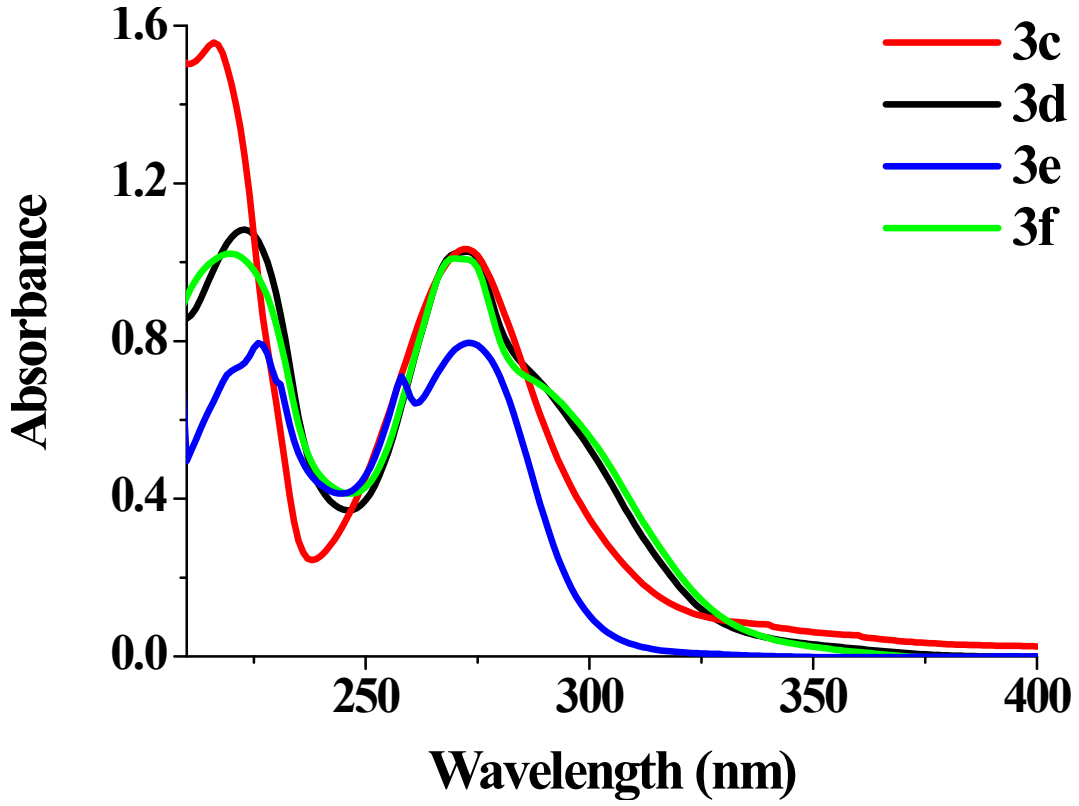

Fig. S3 UV-Vis plot of **3c**, **3d**, **3e** and **3f** at 0.1 mM concentration in acetonitrile

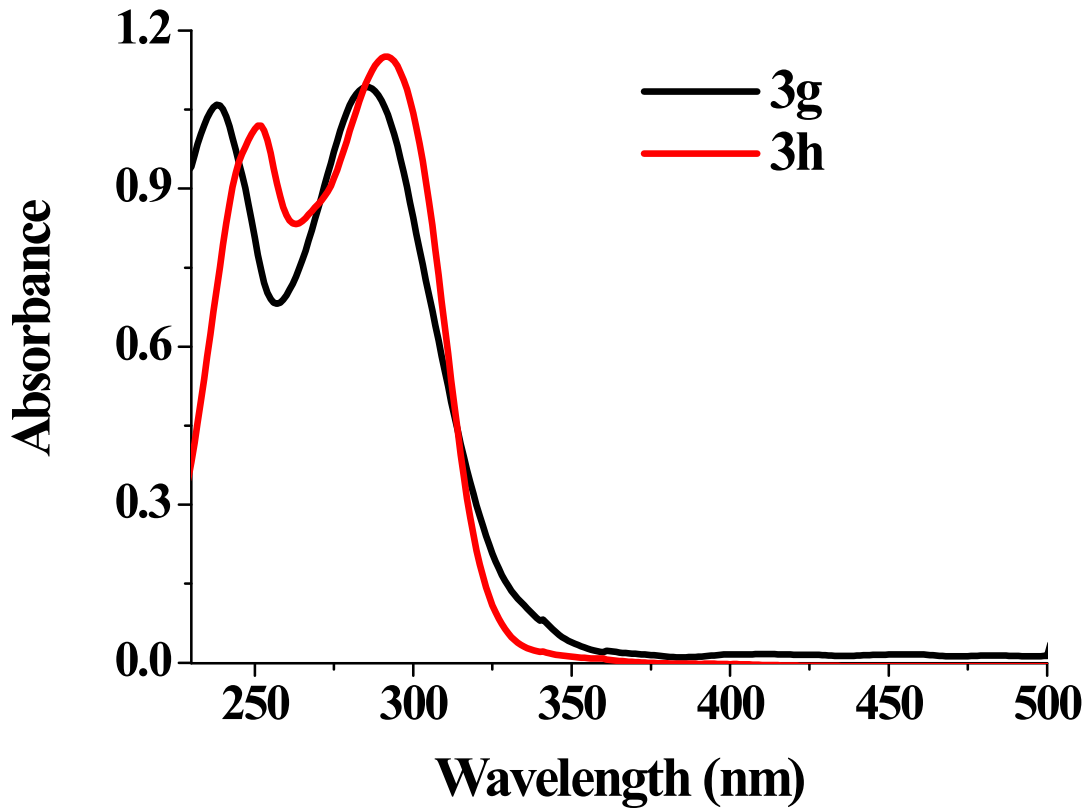

Fig. S4 UV-Vis plot of **3g** and **3h** at 0.1 mM concentration in acetonitrile

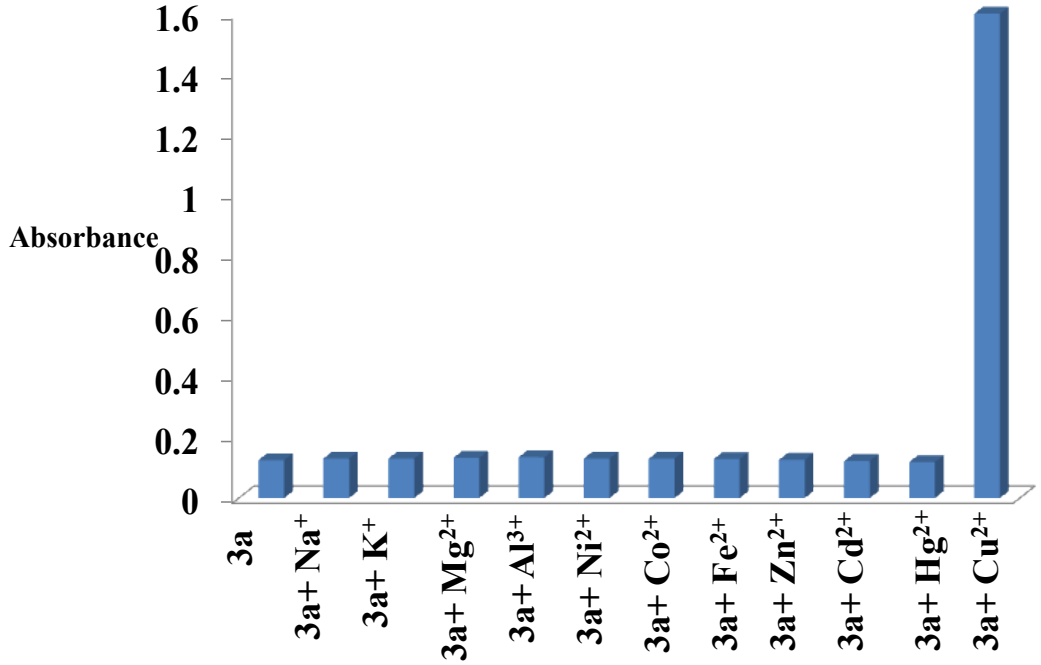

Fig. S5 Chemosensing activity of probe **3a** towards different cationic species (20 equiv.) in acetonitrile

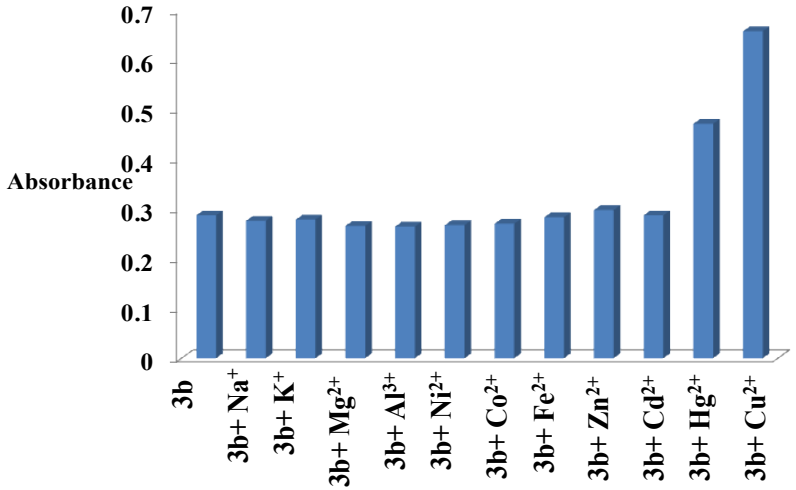
Absorbance
0.7
0.6
0.5
0.4
0.3
0.2
0.1
0
3b
3b+ Na+
3b+ K+
3b+ Mg2+
3b+ Al3+
3b+ Ni2+
3b+ Co2+
3b+ Fe2+
3b+ Zn2+
3b+ Cd2+
3b+ Hg2+
3b+ Cu2+

Fig. S6 Chemosensing activity of probe **3b** towards different cationic species (20 equiv.) in acetonitrile

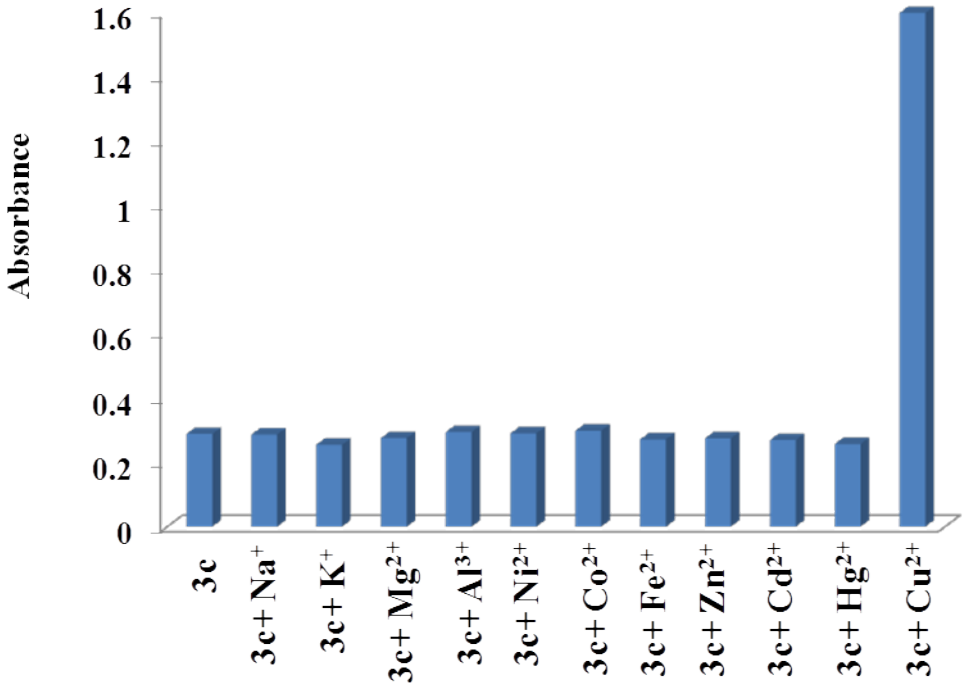

Fig. S7 Chemosensing activity of probe **3c** towards different cationic species (20 equiv.) in acetonitrile

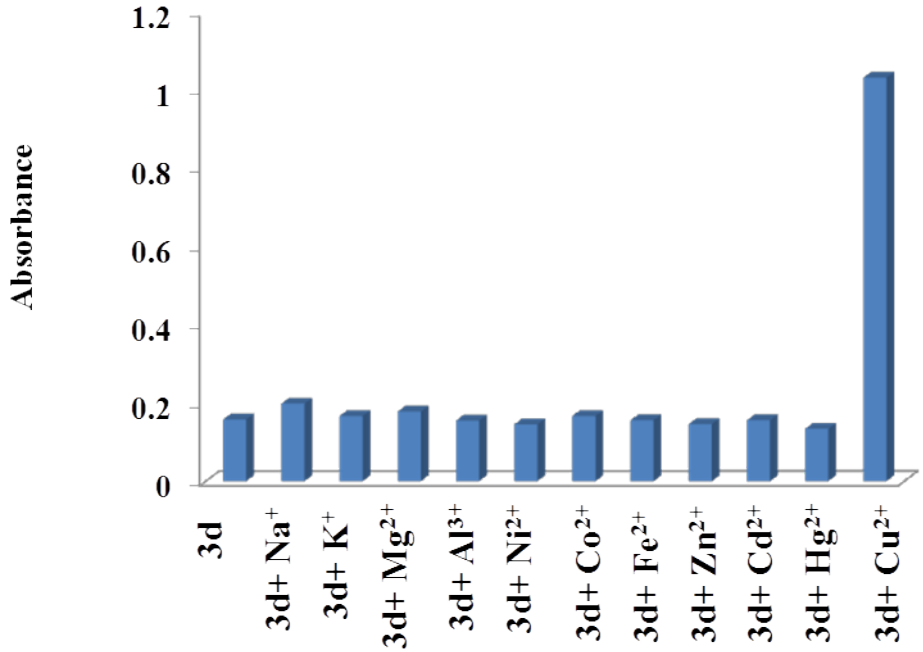

Fig. S8 Chemosensing activity of probe **3d** towards different cationic species (20 equiv.) in acetonitrile

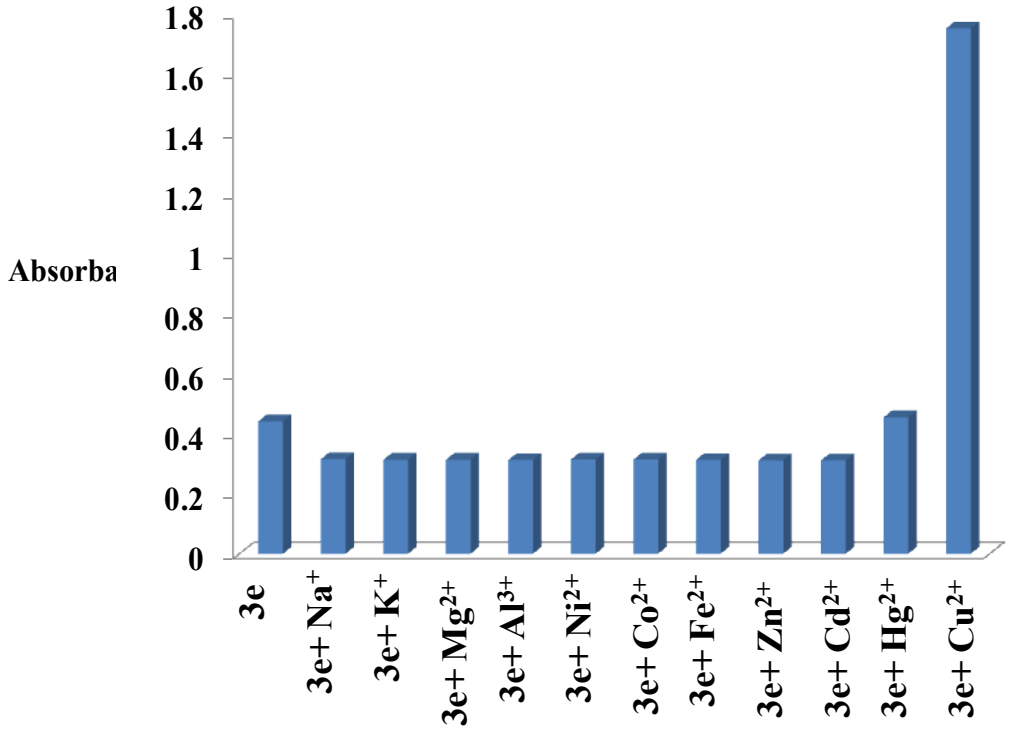

Fig. S9 Chemosensing activity of probe **3e** towards different cationic species (20 equiv.) in acetonitrile

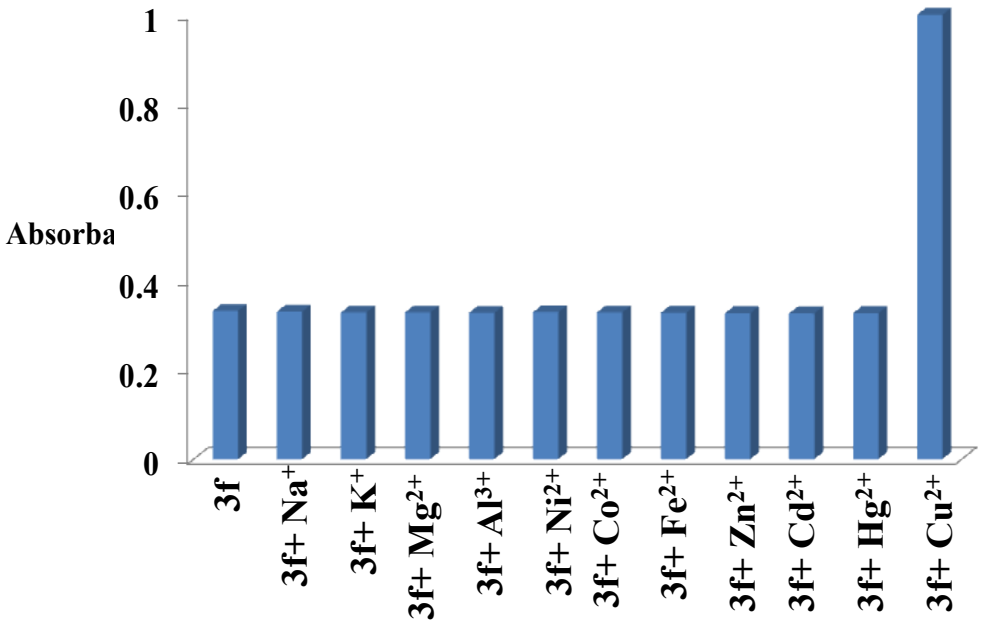

Fig. S10 Chemosensing activity of probe **3g** towards different cationic species (20 equiv.) in acetonitrile

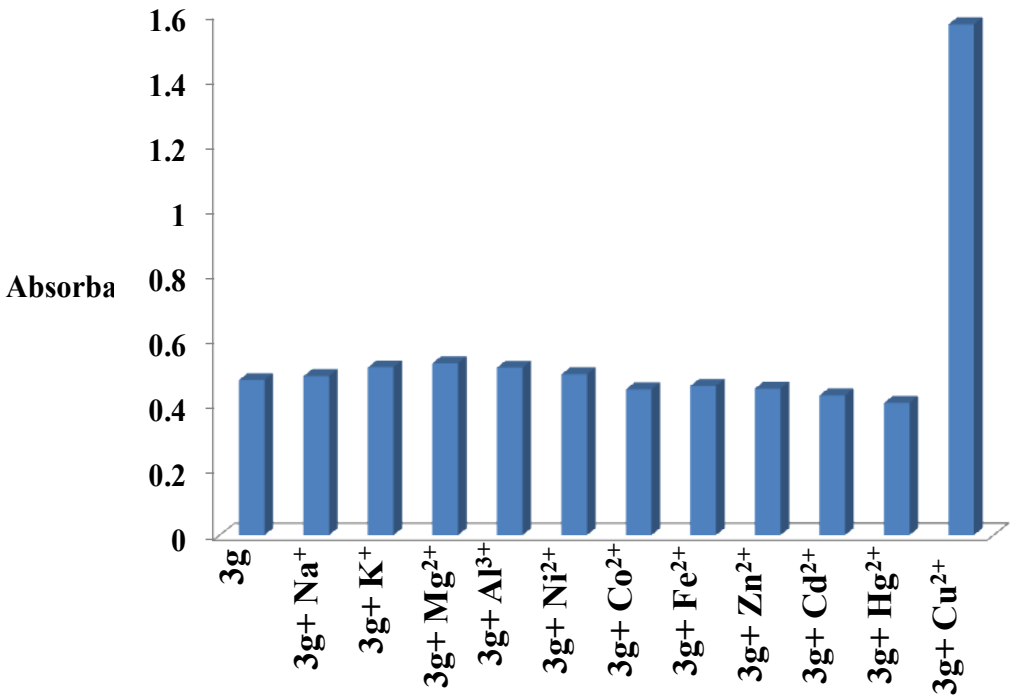

Fig. S11 Chemosensing activity of probe **3g** towards different cationic species (20 equiv.) in acetonitrile

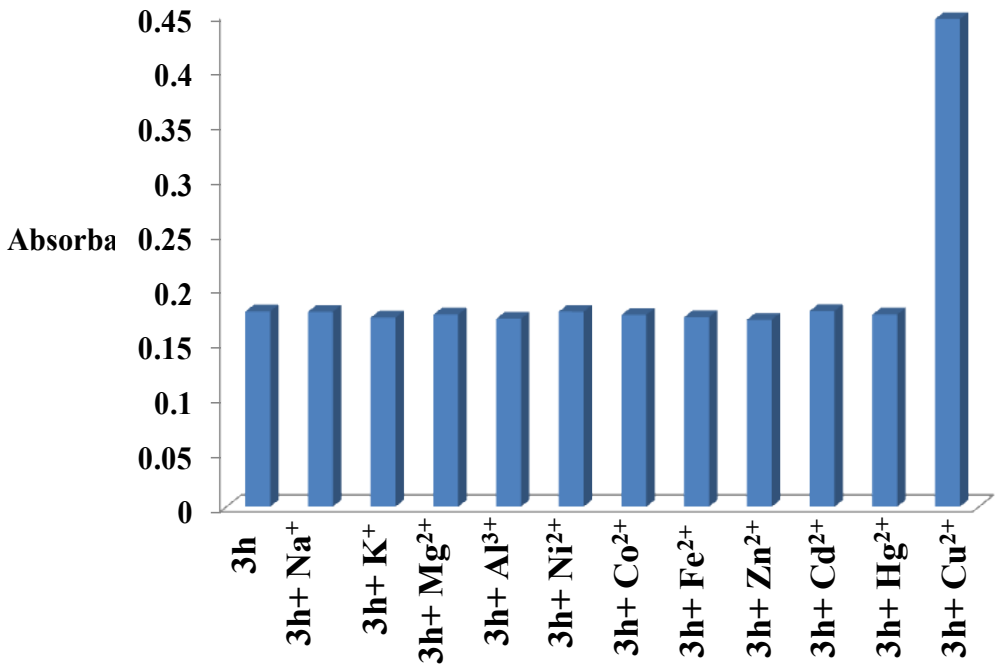

Fig. S12 Chemosensing activity of probe **3h** towards different cationic species (20 equiv.) in acetonitrile

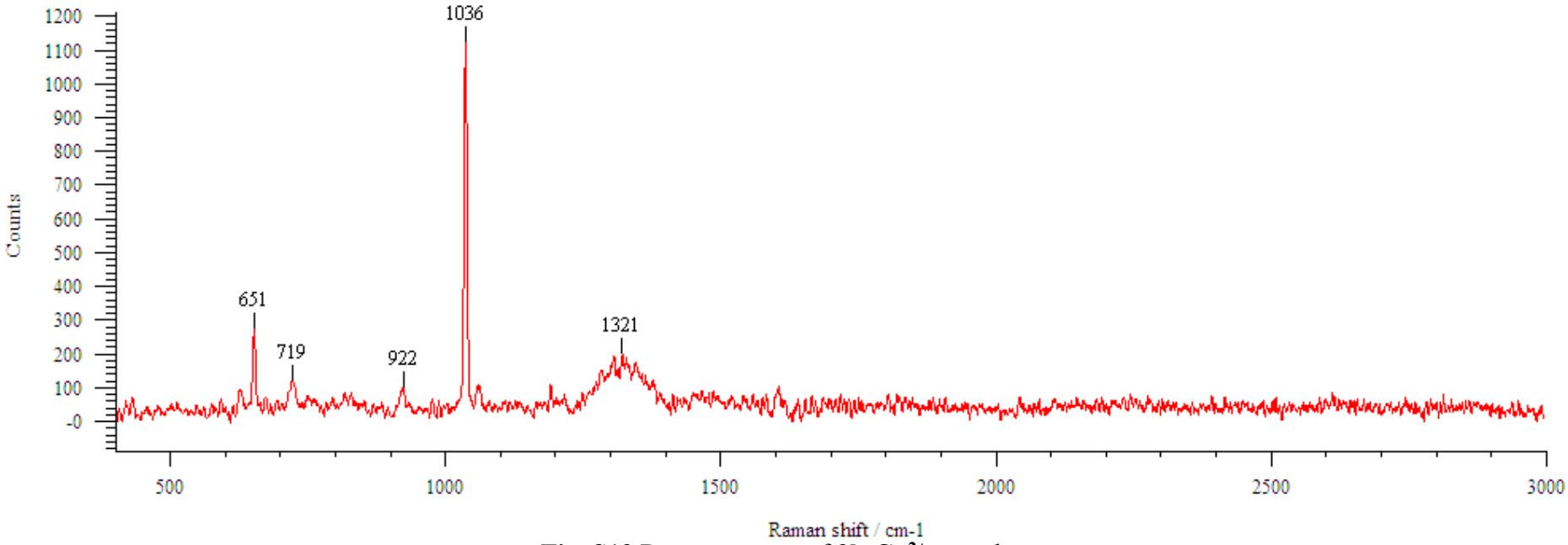

Fig. S13 Raman spectra of **3h·Cu^{2+}** complex

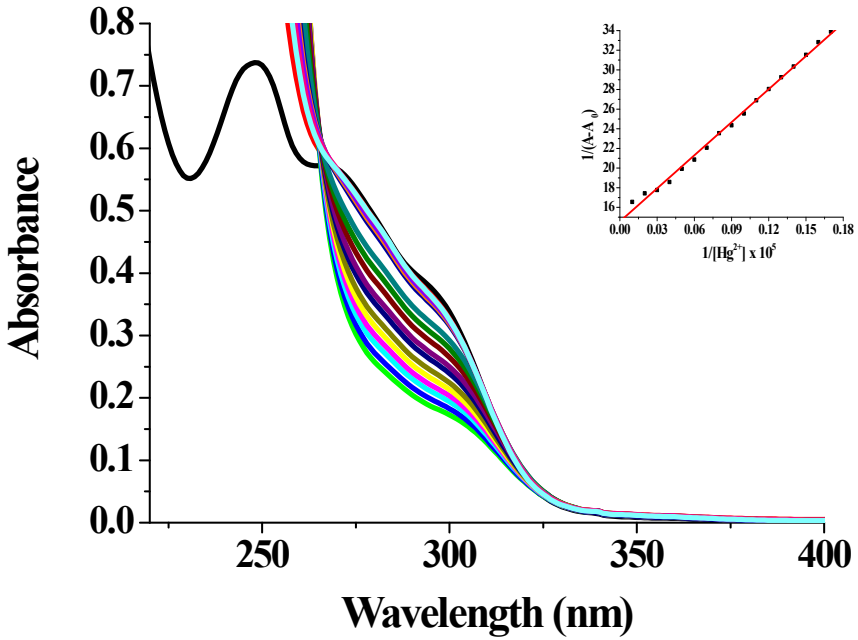

Fig. S14 Family of UV–Vis spectra taken in the course of the titration of **3b** (1 μM in CH_3CN) with Hg^{2+} ions (0-5 equiv. (0-5 equiv.i.e. 0, 0.3, 0.6, 0.9, 1.2, 1.4. 1.5, 1.8, 2.1, 2.4, 2.7, 3, 4, 5 in the increasing order).). Inset shows the B-H plot for 1:1 complexation between **3b** and Hg^{2+} at 266 nm (R = .9979) and $K_a = 3.95 \times 10^5\ M^{-1}$

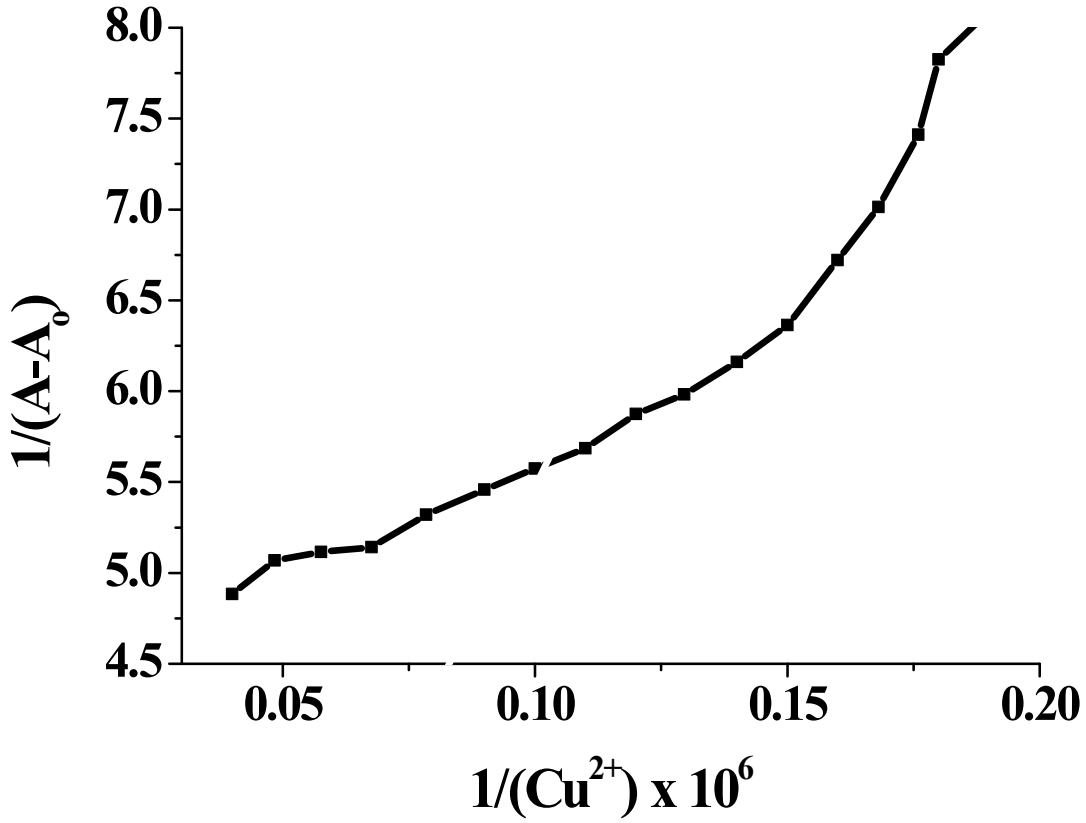

Fig. S15 B-H plot for 1:1 complexation between **3e** and Cu^{2+} at 296 nm

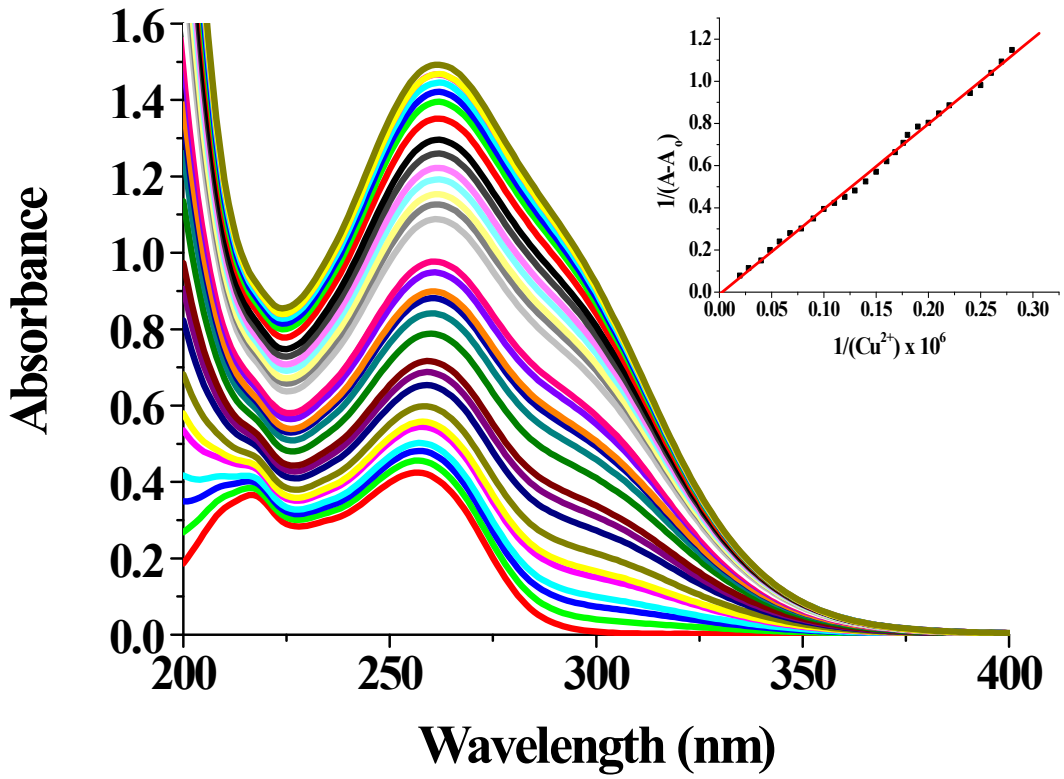

Fig. S16 Family of UV–Vis spectra taken in the course of the titration of **3a** (1 μM in CH_3CN) with Cu^{2+} ions (0-10 equiv. 0, 0.4, 0.8, 1.2, 1.6, 2.0, 2.4, 2.8, 3.2, 3.6, 4.0, 4.4, 4.8, 5.2, 5.6, 6.0, 6.4, 6.8, 7.2, 7.6, 8.0, 8.4, 8.8, 9.2, 9.6, 10.0). Inset shows the B-H plot for 1:1 complexation between **3a** and Cu^{2+} at 261 nm (R = 0.9929)

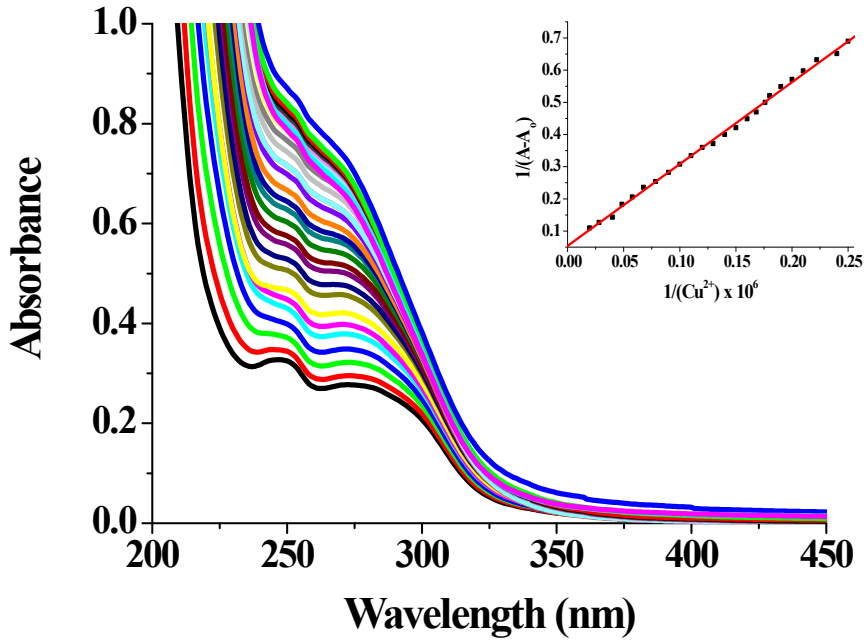

Fig. S17 Family of UV–Vis spectra taken in the course of the titration of **3b** (1 μM in CH_3CN) with Cu^{2+} ions (0-4 equiv. i.e. 0, 0.2, 0.4, 0.6, 0.8, 1.0, 1.2, 1.4, 1.6, 1.8, 2.0, 2.2, 2.4, 2.6, 2.8, 3.0, 3.2, 3.4, 3.6, 3.8, 4.0). Inset shows the B-H plot for 1:1 complexation between **3b** and Cu^{2+} ion at 292nm (R = 0.9987)

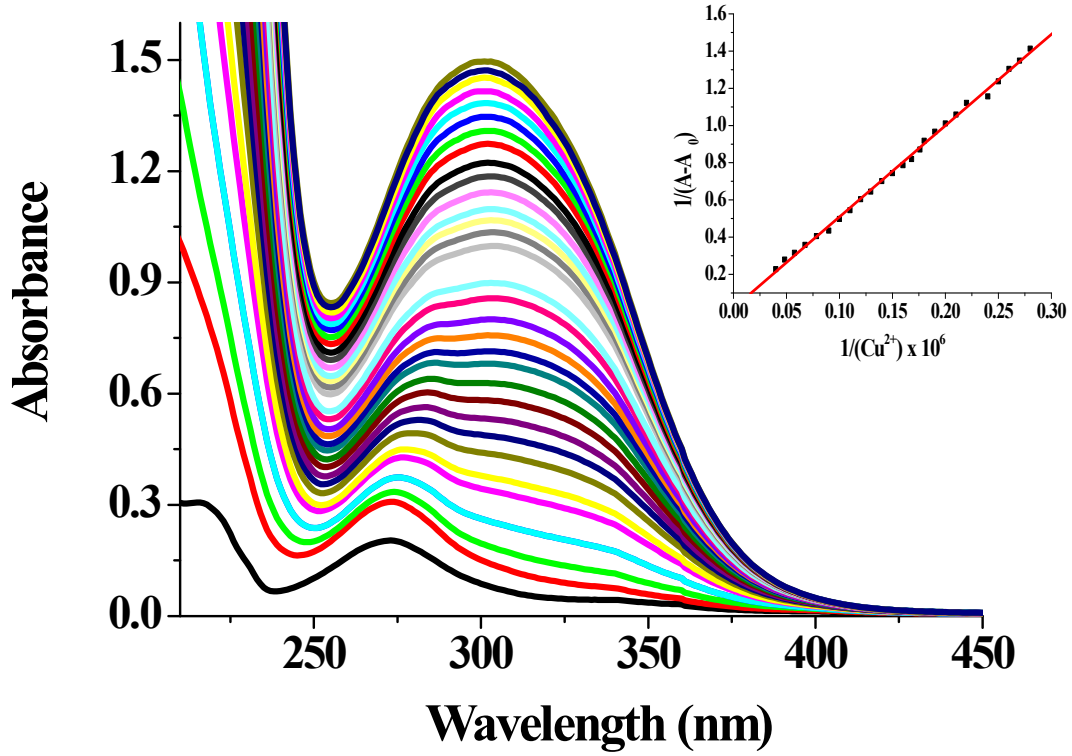

Fig. S18 Family of UV–Vis spectra taken in the course of the titration of **3c** (1 μM in CH_3CN) with Cu^{2+} ions (0-4 equiv. i.e. 0, 0.2, 0.4, 0.6, 0.8, 1.0, 1.2, 1.4, 1.6, 1.8, 2.0, 2.2, 2.4, 2.6, 2.8, 3.0, 3.2, 3.4, 3.6, 3.8, 4.0). Inset shows the B-H plot for 1:1 complexation between **3c** and Cu^{2+} at 302 nm (R = 0.9989)

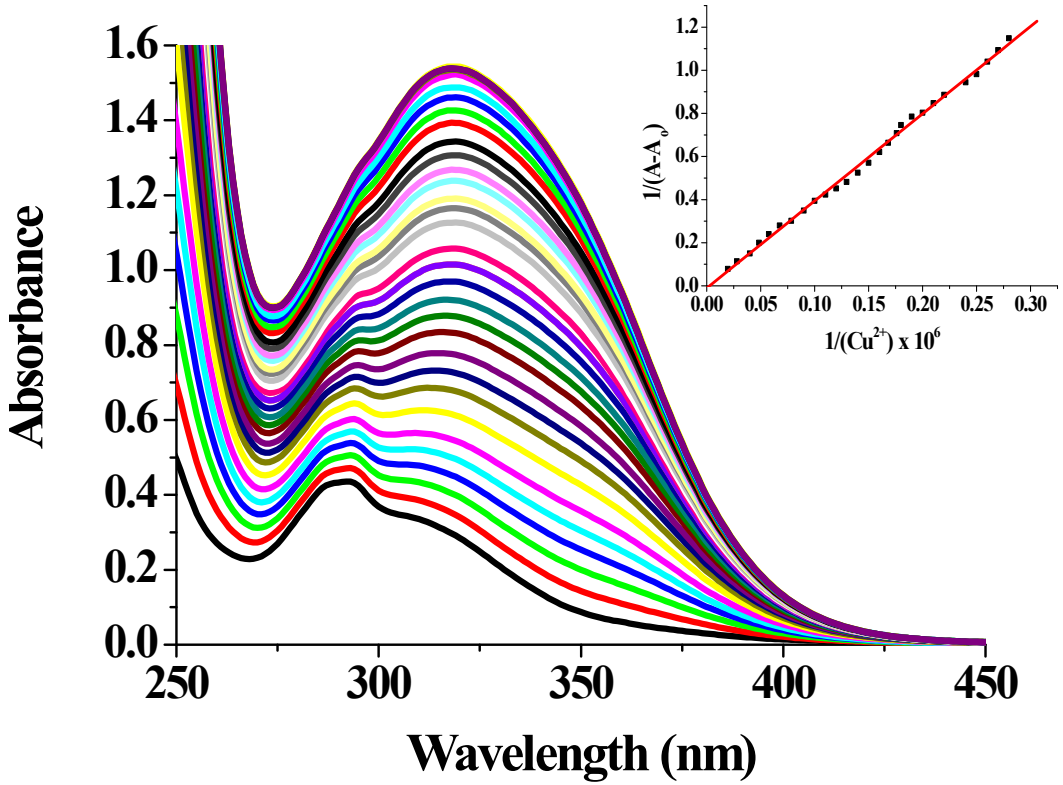

Fig. S19 Family of UV–Vis spectra taken in the course of the titration of **3d** (1 μM in CH_3CN) with Cu^{2+} ions (0-4 equiv. i.e. 0, 0.2, 0.4, 0.6, 0.8, 1.0, 1.2, 1.4, 1.6, 1.8, 2.0, 2.2, 2.4, 2.6, 2.8, 3.0, 3.2, 3.4, 3.6, 3.8, 4.0). Inset shows the B-H plot for 1:1 complexation between **3d** and Cu^{2+} at 300 nm (R = 0.9987)

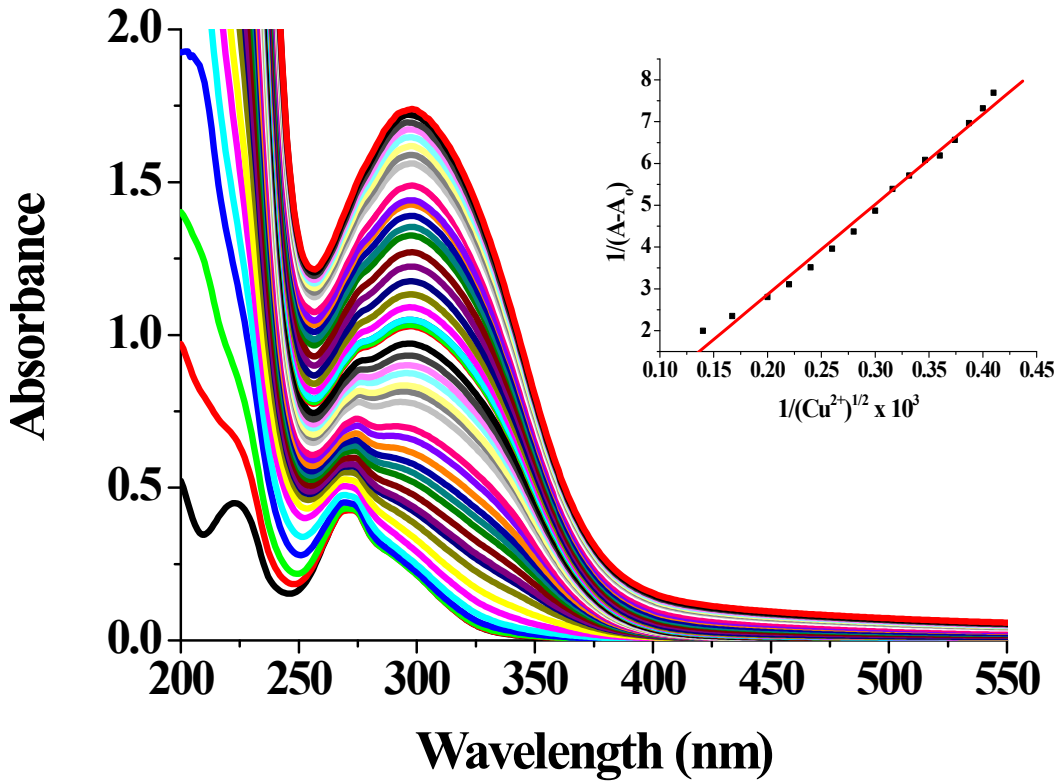

Fig. S20 Family of UV–Vis spectra taken in the course of the titration of **3e** (1 μM in CH_3CN) with Cu^{2+} ions (0-10 equiv. i.e. 0, 0.3, 0.6, 0.9, 1.2, 1.5, 1.8, 2.1, 2.4, 2.7, 3.0, 3.3, 3.6, 3.9, 4.2, 4.5, 4.8, 5.1, 5.4, 5.7, 6.0, 6.3, 6.6, 6.9, 7.2, 7.5, 7.8, 8.1, 8.4, 8.7, 9, 10). Inset shows the B-H plot for 1:0.5 complexation between **3e** and Cu^{2+} at 296 nm (R = 0.9923).

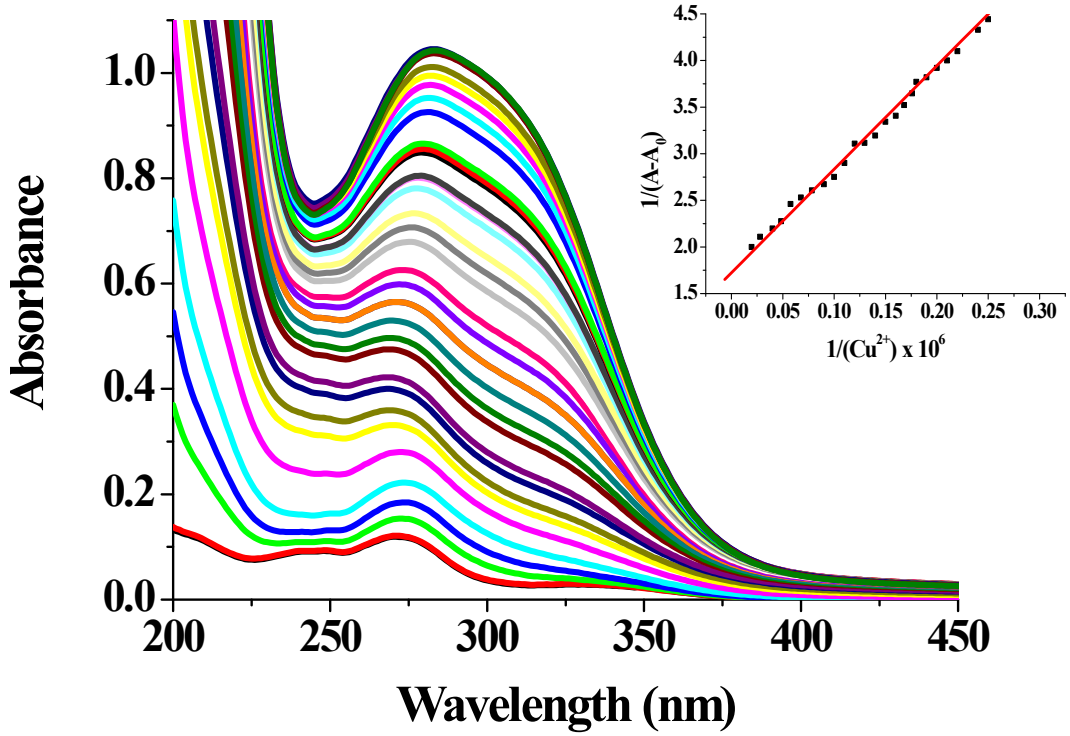

Fig. S21 Family of UV–Vis spectra taken in the course of the titration of **3f** (1 μM in CH_3CN) with Cu^{2+} ions (0-10 equiv. i.e. 0, 0.4, 0.8, 1.2, 1.6, 2.0, 2.4, 2.8, 3.2, 3.6, 4.0, 4.4, 4.8, 5.2, 5.6, 6.0, 6.4, 6.8, 7.2, 7.6, 8.0, 8.4, 8.8, 9.2, 9.6, 10.0). Inset shows the B-H plot for 1:1 complexation between **3f** and Cu^{2+} at 283 nm (R = 0.9978)

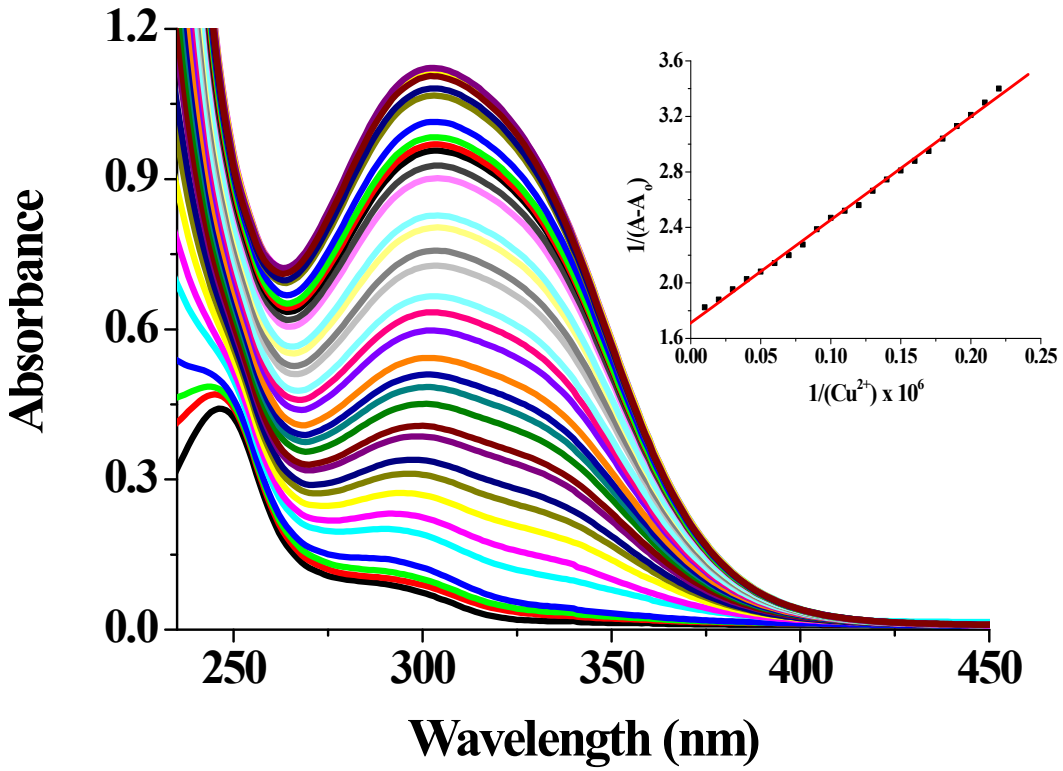

Fig. S22 Family of UV–Vis spectra taken in the course of the titration of **3g** (1 μM in CH_3CN) with Cu^{2+} ions (0-4 equiv. i.e. 0, 0.2, 0.4, 0.6, 0.8, 1.0, 1.2, 1.4, 1.6, 1.8, 2.0, 2.2, 2.4, 2.6, 2.8, 3.0, 3.2, 3.4, 3.6, 3.8, 4.0). Inset shows the B-H plot for 1:1 complexation between **3g** and Cu^{2+} at 318 nm (R = 0.9879)

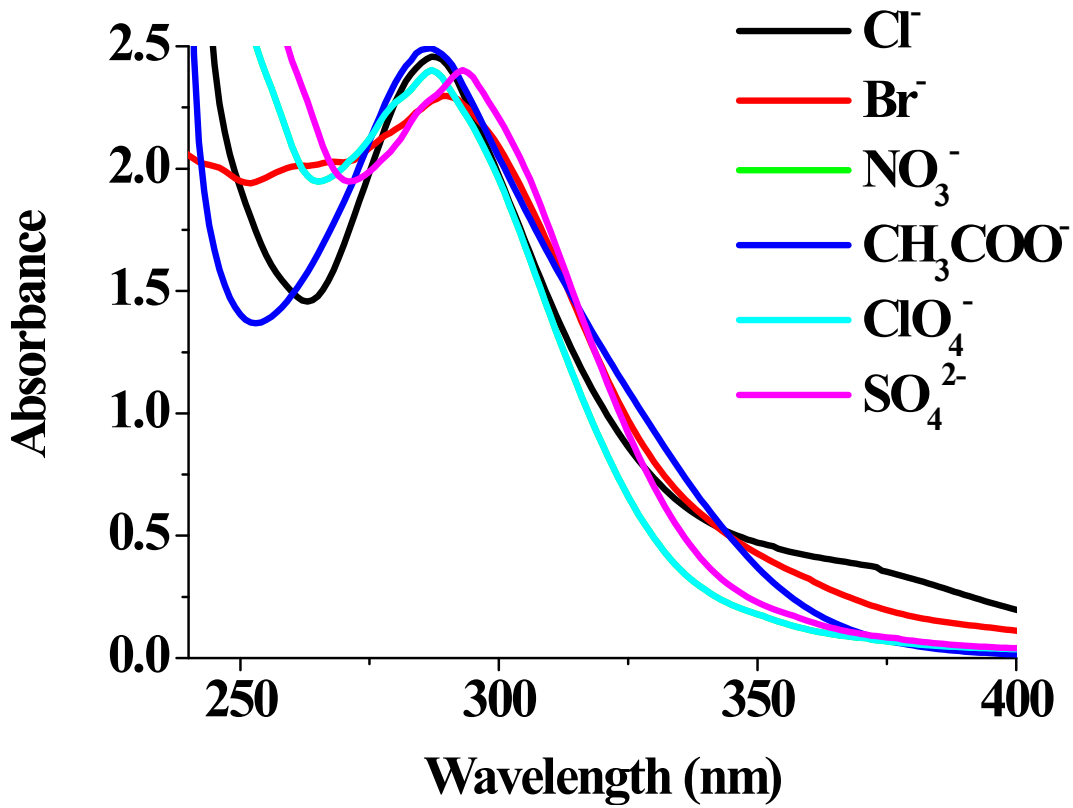

Fig. S23 UV-Vis absorption spectra of **3h** in the presence of CuX_2 (where X = Cl^-, Br^-, NO_3^-, CH_3COO^-, ClO_4^-, SO_4^{2-})

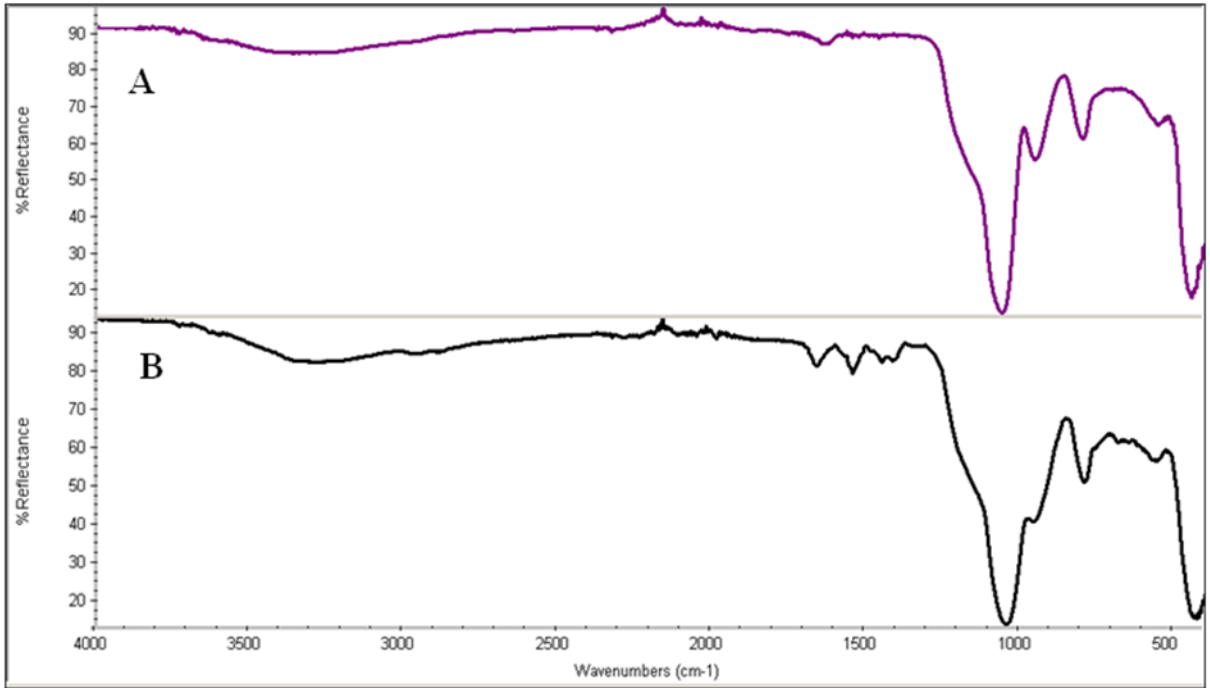

Fig. S24 IR spectra of SiNPs (A) and H-SiNPs (B)

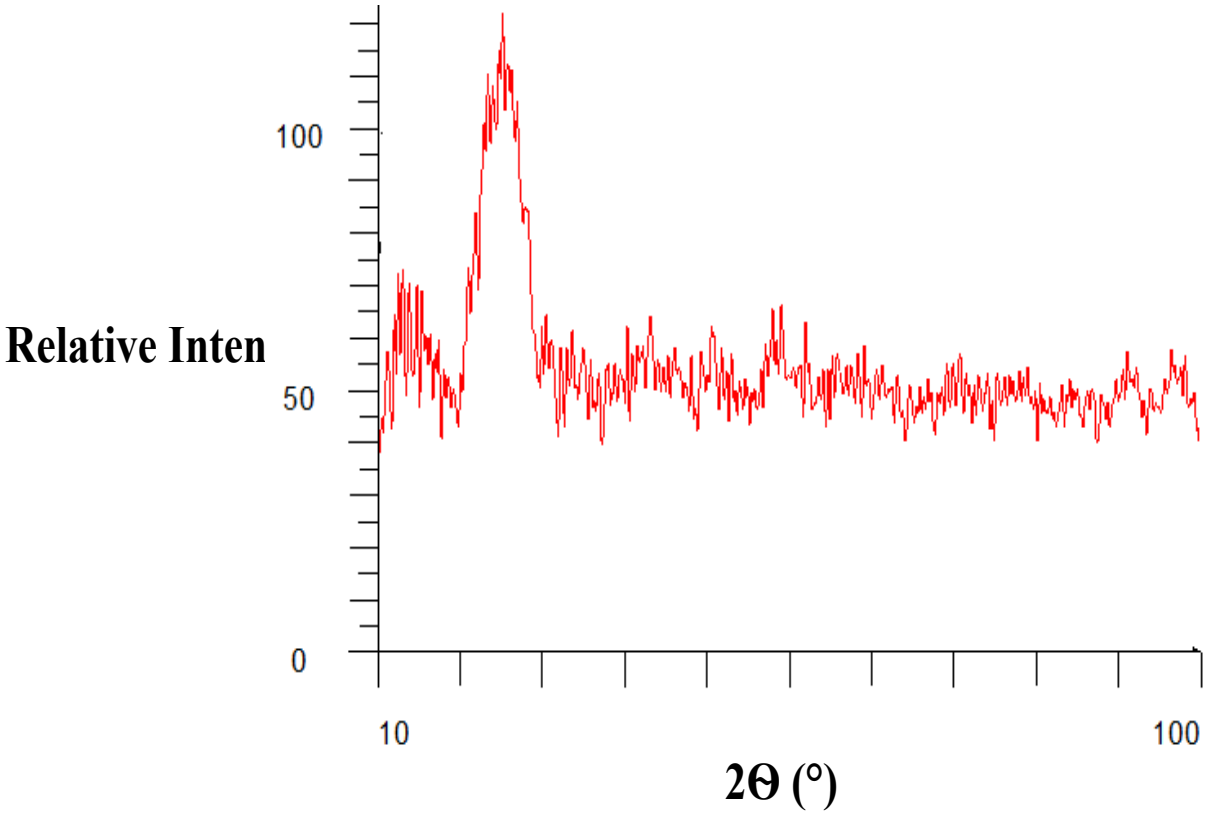

Fig. S25 X-ray diffraction (XRD) graphs of SiNPs (A) and H-SiNPs (B)

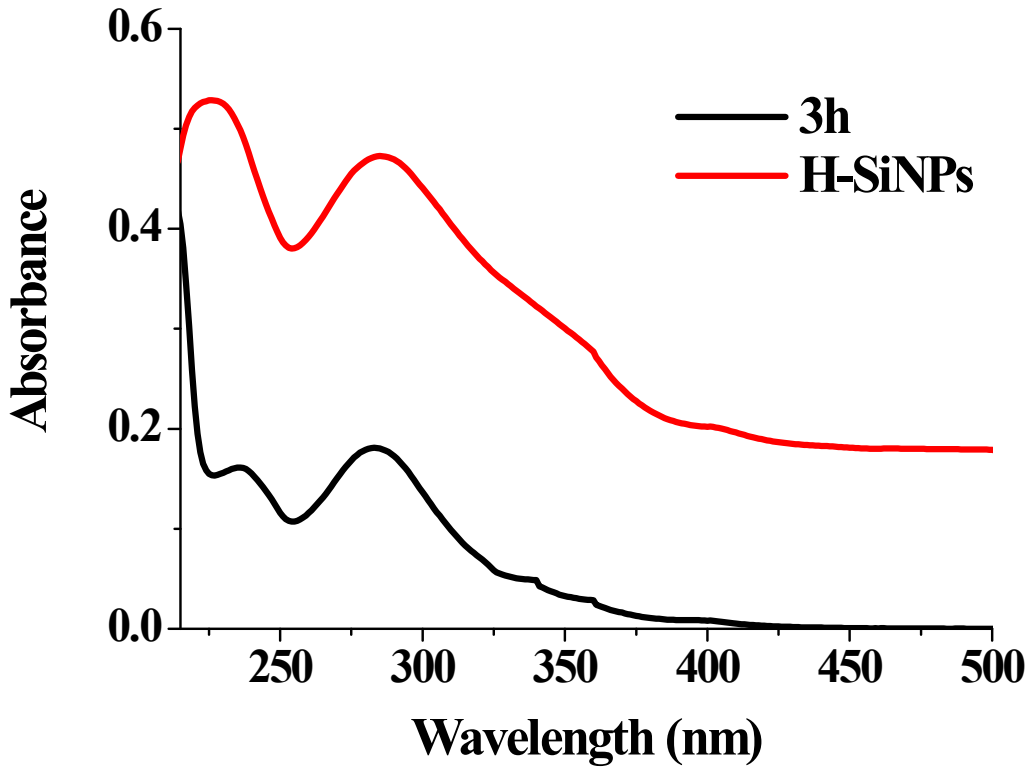

Fig. S26 UV-Vis plot of **3h** and **H-SiNPs** in acetonitrile

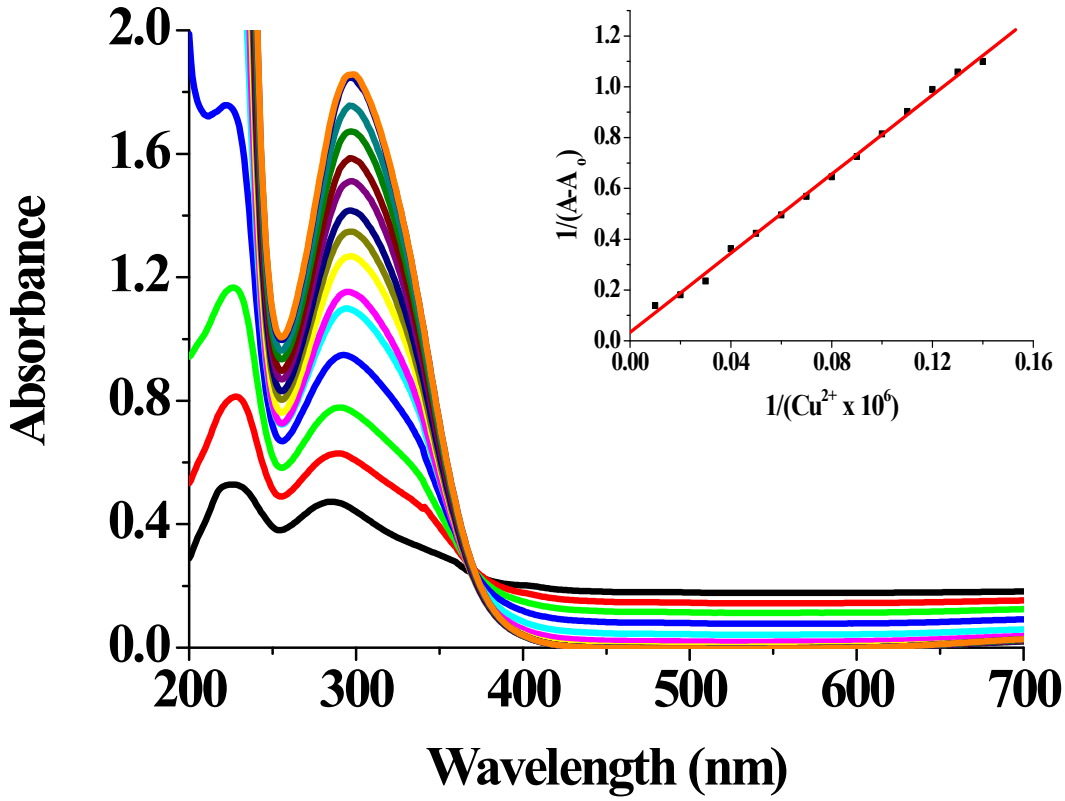

Fig. S27 Family of UV–Vis spectra taken in the course of the titration of **H-SiNPs** (in CH_3CN) with Cu^{2+} ions. Inset shows the B-H plot for 1:1 complexation between **H-SiNPs** and Cu^{2+} at 297nm (R = 0.9955)

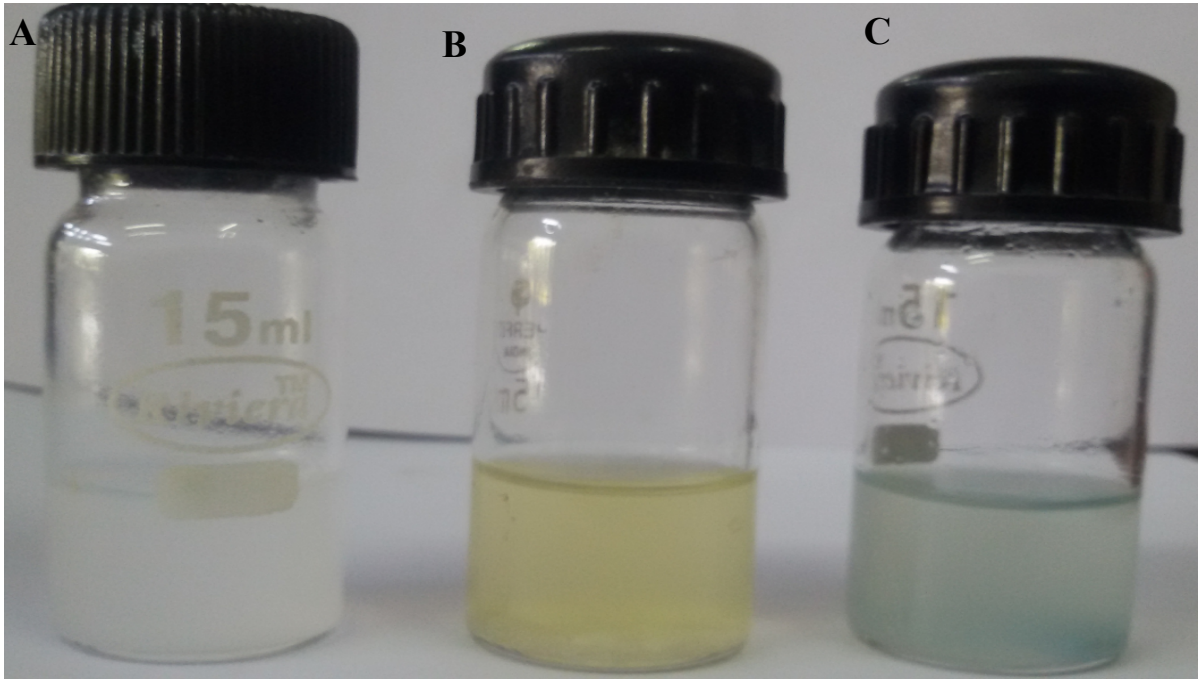

Fig. S28 Digital photographs of aqueous dispersions of SiNPs (A), H-SiNPs (B) and Cu^{2+}·H-SiNPs complex (C)

Table T1 Selected crystal data and details on the structure determinations from single crystal data for compound **3e**

Compound	**3e**
Formula	$C_{15}H_{22}N_2O_4SSi$
MW [g·mol^{-1}]	354.49
Crystal system	Monoclinic
Space group	$P12_1/n1$
a [Å]	11.5580(1)
b [Å]	7.3752(7)
c [Å]	19.4783(2)
α [deg]	90
β [deg]	93.613(3)
γ [deg]	90
V [Å^3]	1657.1(3)
T [K]	170.15
Z	4

ρ_{calc} [g·cm^{-3}]	1.421
μ [mm^{-1}]	0.289
Min/max transmission	0.961/0.977
θ_{max} [deg]	28.370
Measured reflections	27042
Unique reflections	4117
Reflections [$F_0 > 4\square(F_0)$]	2944
Parameter	208
R_{int}	0.0713
R_1 [$F_0 > 4\square(F_0)$]	0.0409
wR_2 [all data]	0.0978
GOF	1.018
$\Delta\rho_{max}/\Delta\rho_{min}$ [e·Å^{-3}]	0.300/-0.379

Table T2 Comparison of different sensing systems bearing ‘thio’ functionality for the detection of metal ions

Sensors	Sensing metals	Binding constants (M^{-1})	Stoichiometry	Reference
Thio-urea conjugated 1,8-naphthalimide	Fe^{3+}	1.854×10^3	1:1	42 (a)
Thio-urea conjugated pyrene	Cu^{2+}	1.09×10^4	1:1	42 (b)
Thio-spirolactam conjugated rhodamine	Hg^{2+}	1.82×10^5	1:1	42 (c)
Thio-semicarbazide conjugated naphthalimide	Ag+	4.80×10^4	1:1	42 (d)
thio- β-enaminone analog	Cu^{2+}	1.10×10^4	1:1	13
Bis (thio-ester) framed silatrane (3h)	**Cu^{2+}**	4.93×10^5	**1:1**	**Present work**

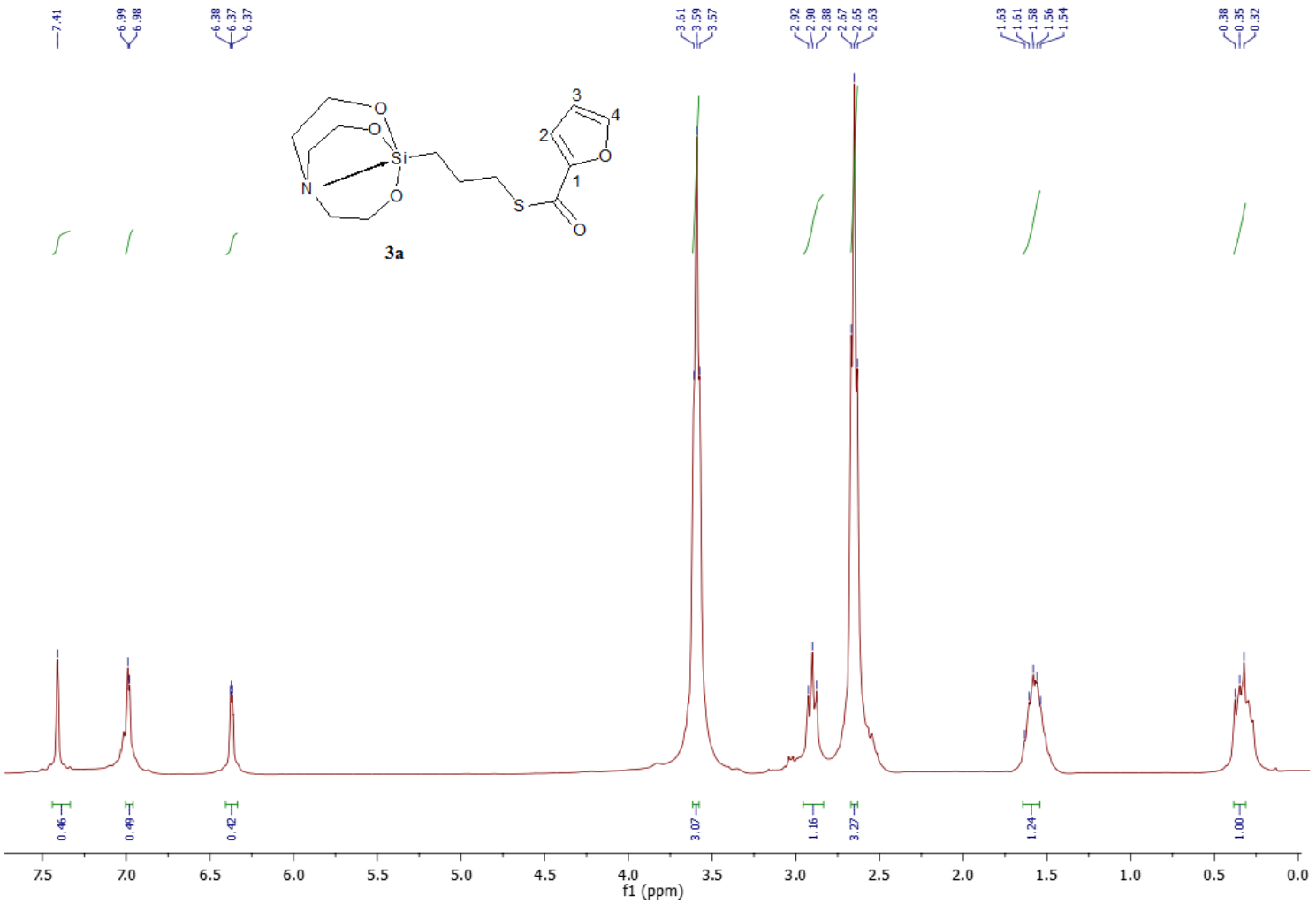

Fig. S29 ^{1}H NMR spectrum of **3a**

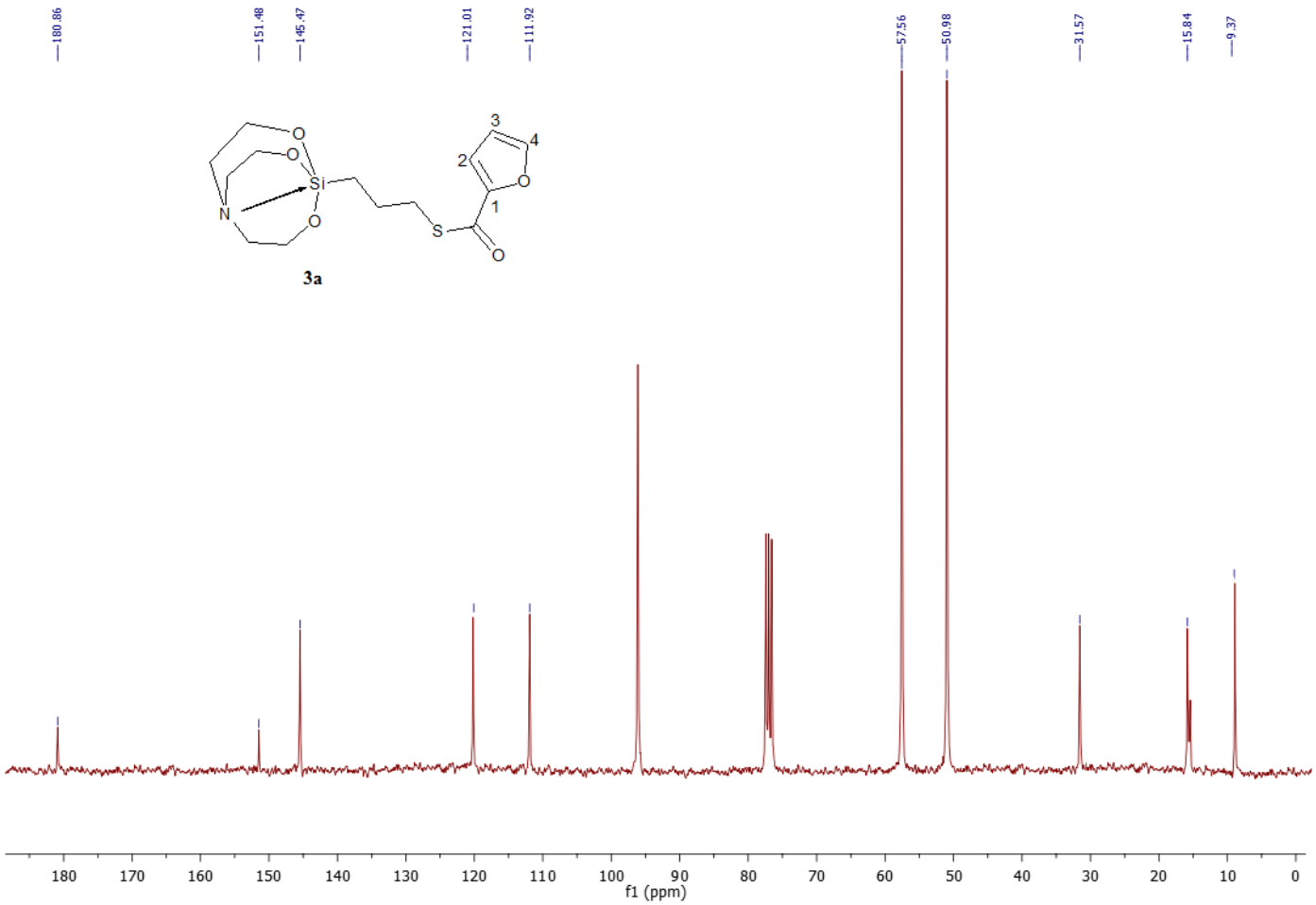

Fig. S30 ^{13}C NMR spectrum of **3a**

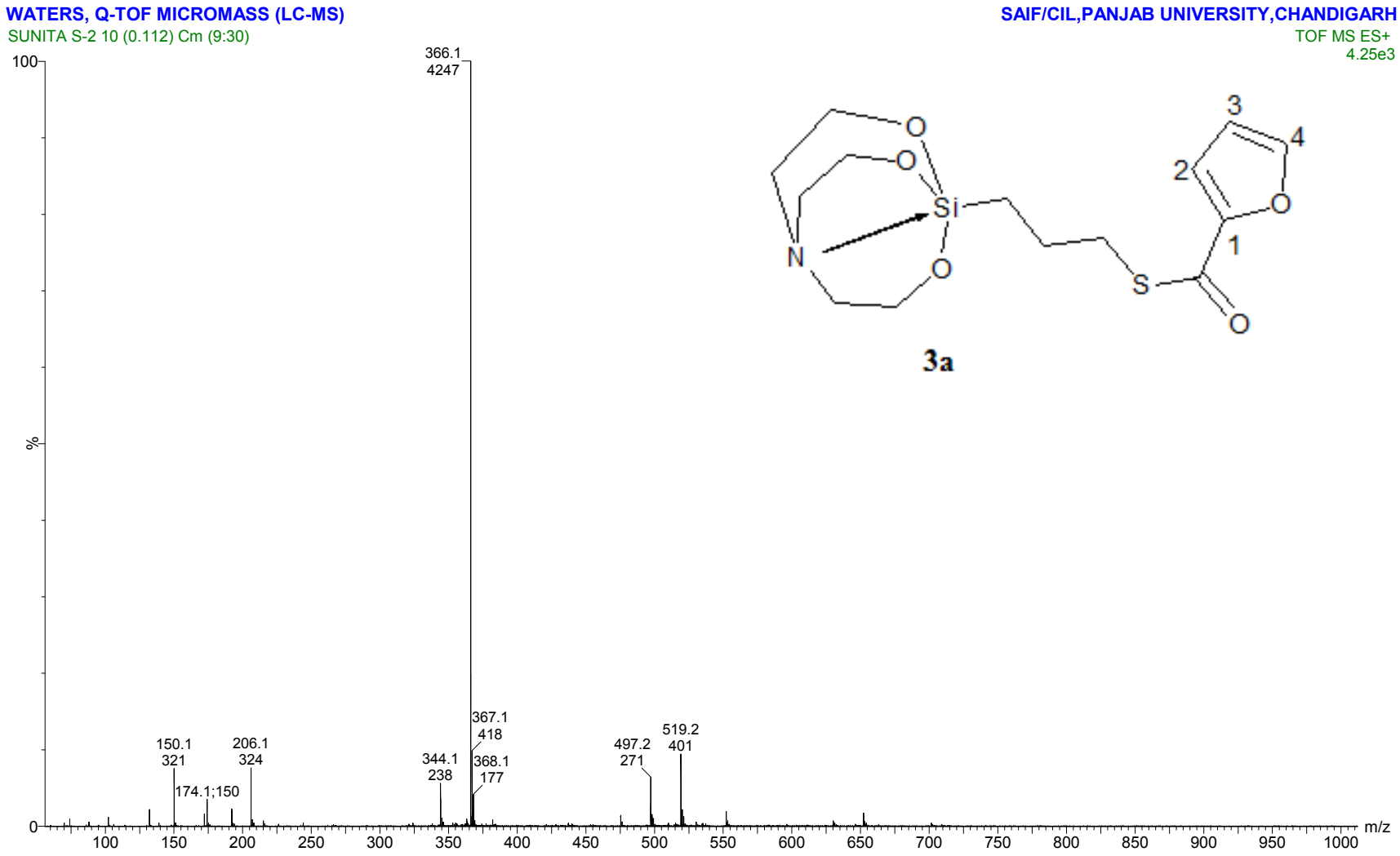

Fig. S31 Mass spectrum of **3a**

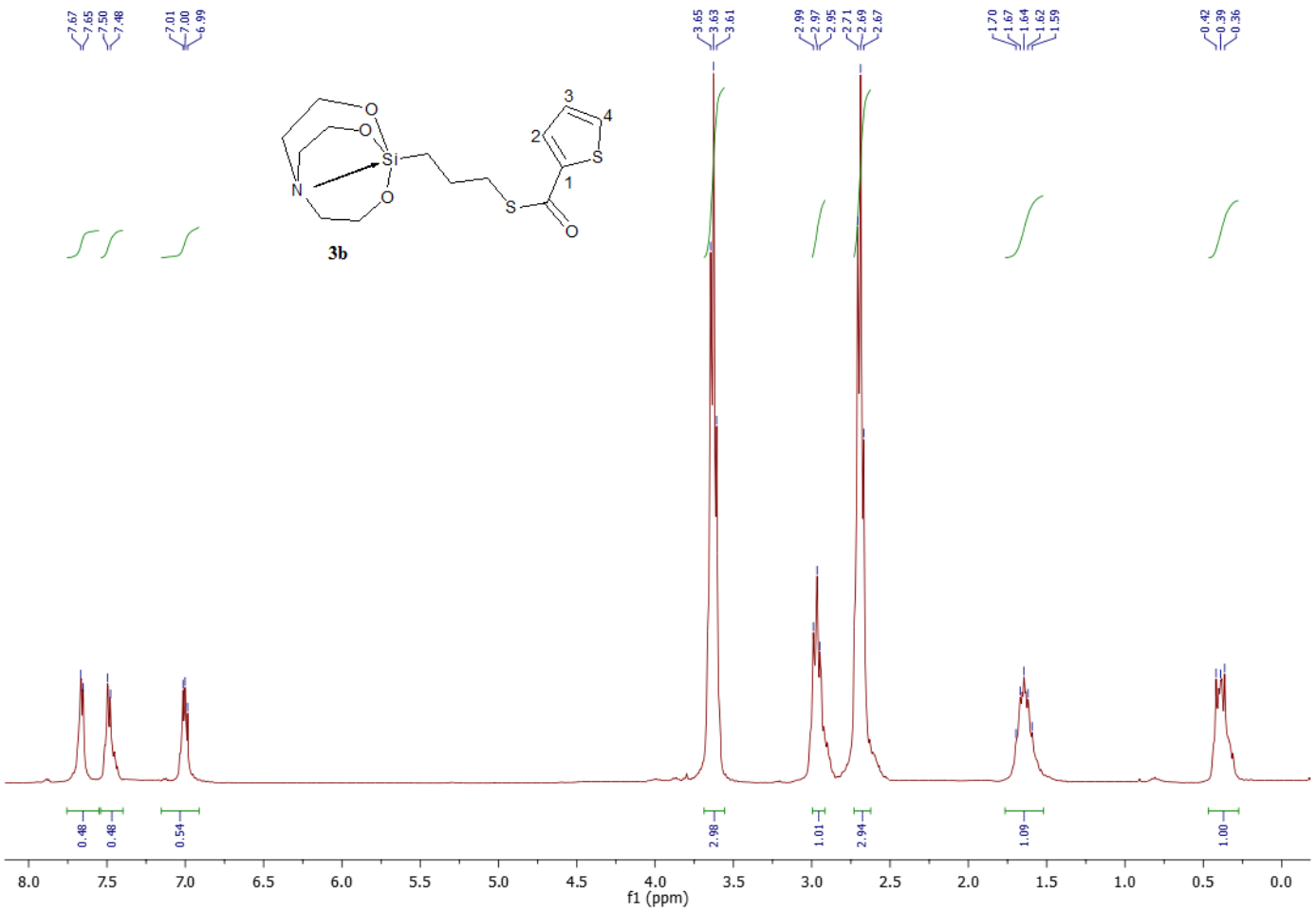

Fig. S32 ^{1}H NMR spectrum of **3b**

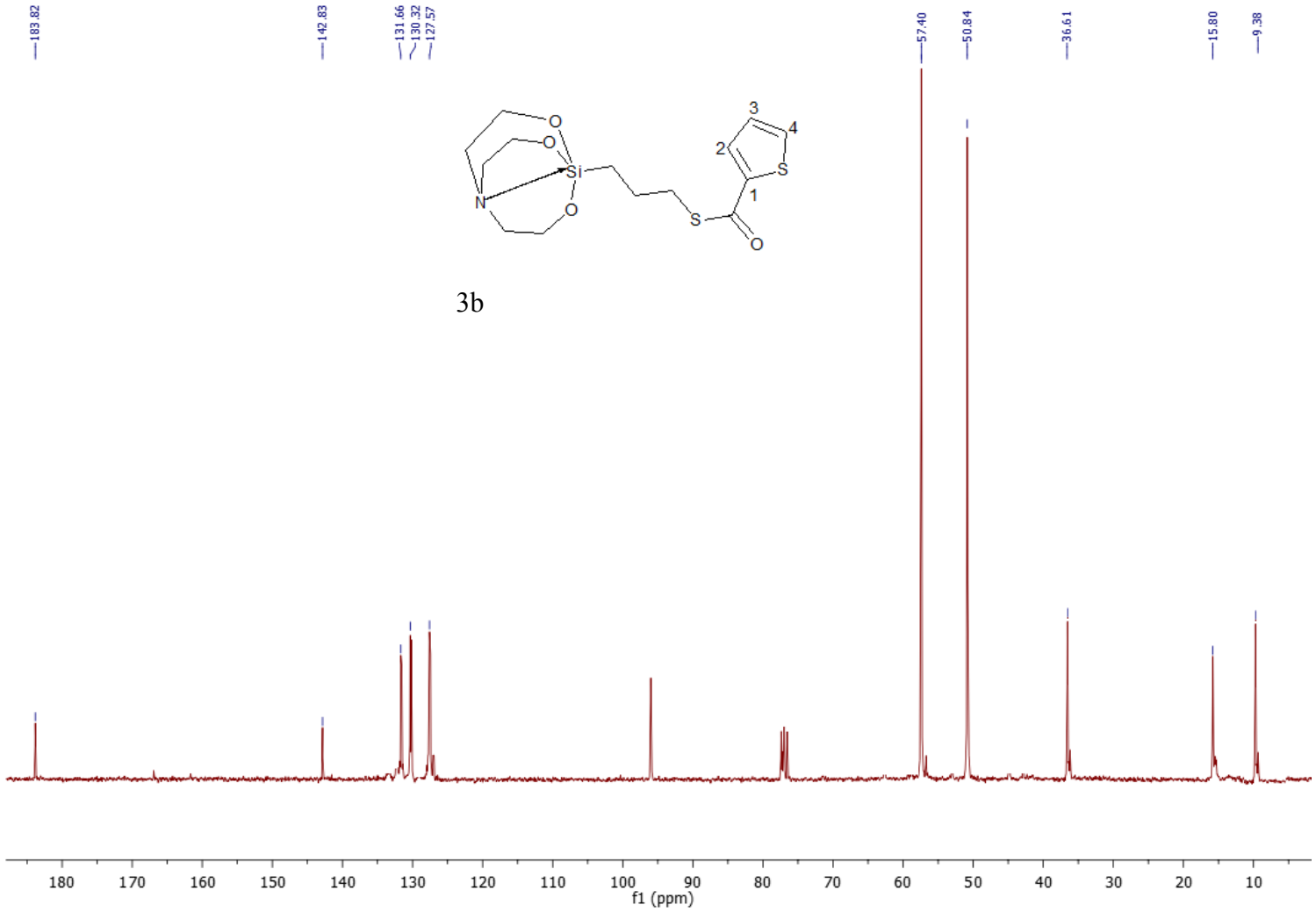

3b

Fig. S33 ^{13}C NMR spectrum of **3b**

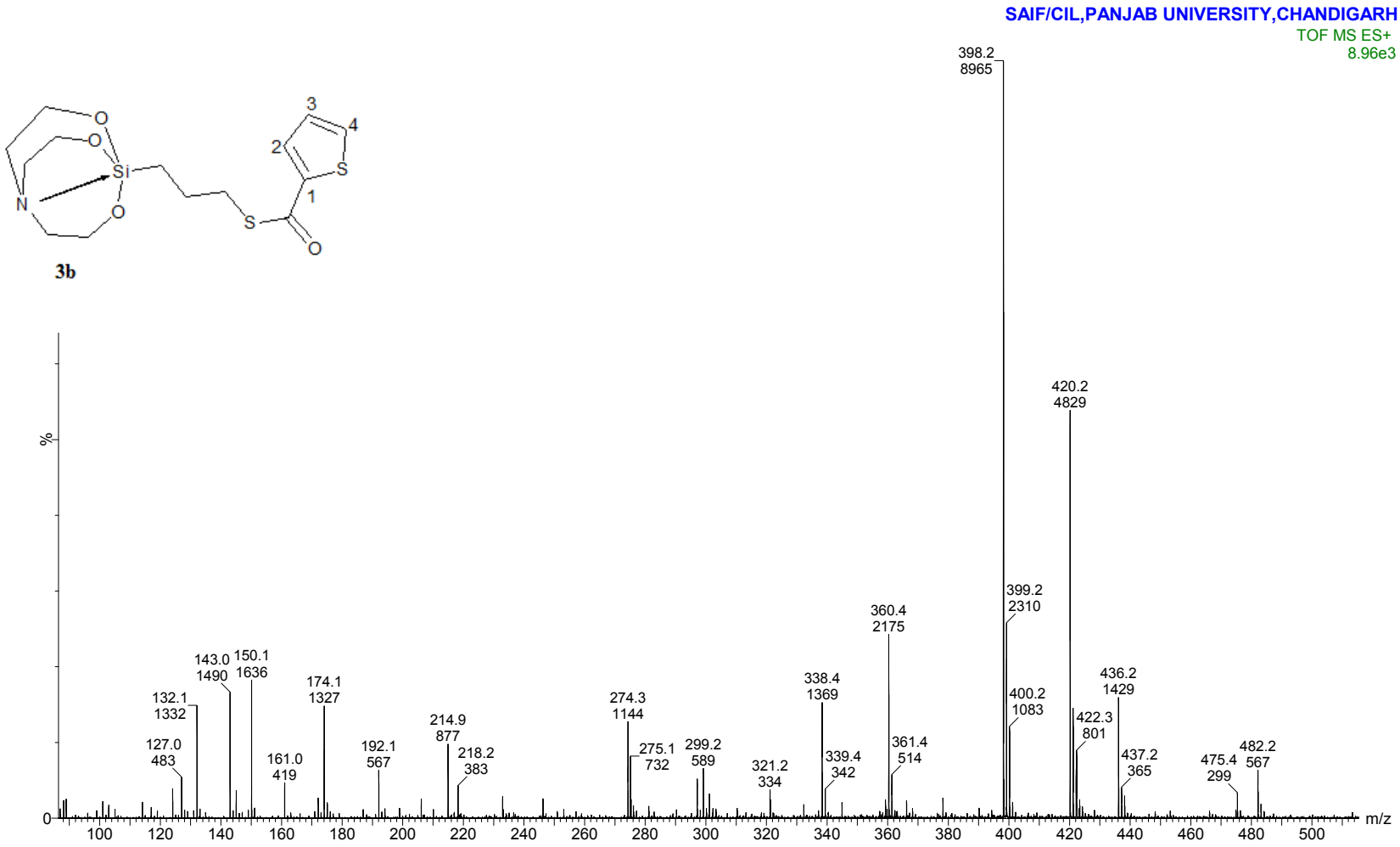

Fig. S34 ^{1}H NMR spectrum of **3b**

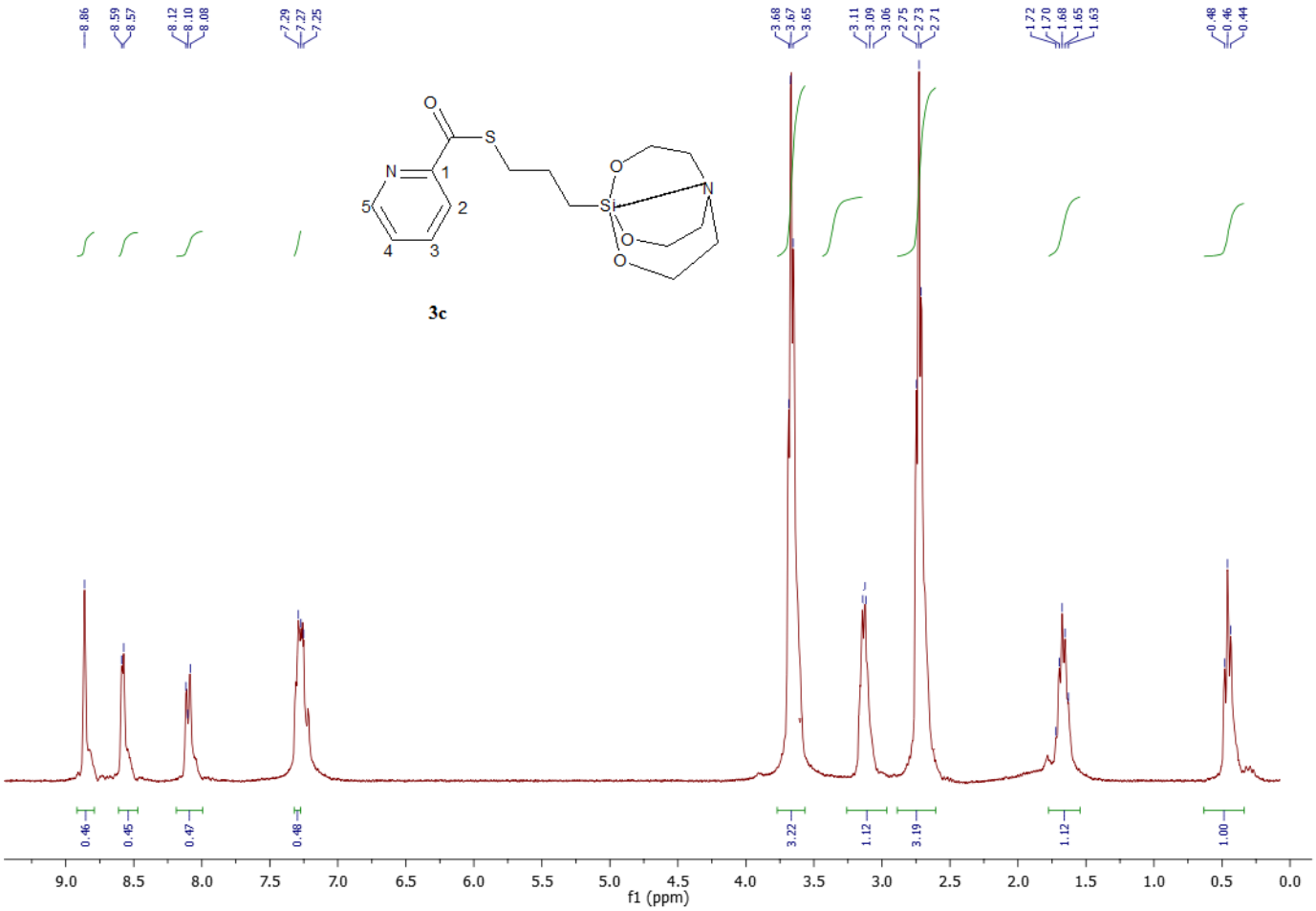

Fig. S35 ^{1}H NMR spectrum of **3c**

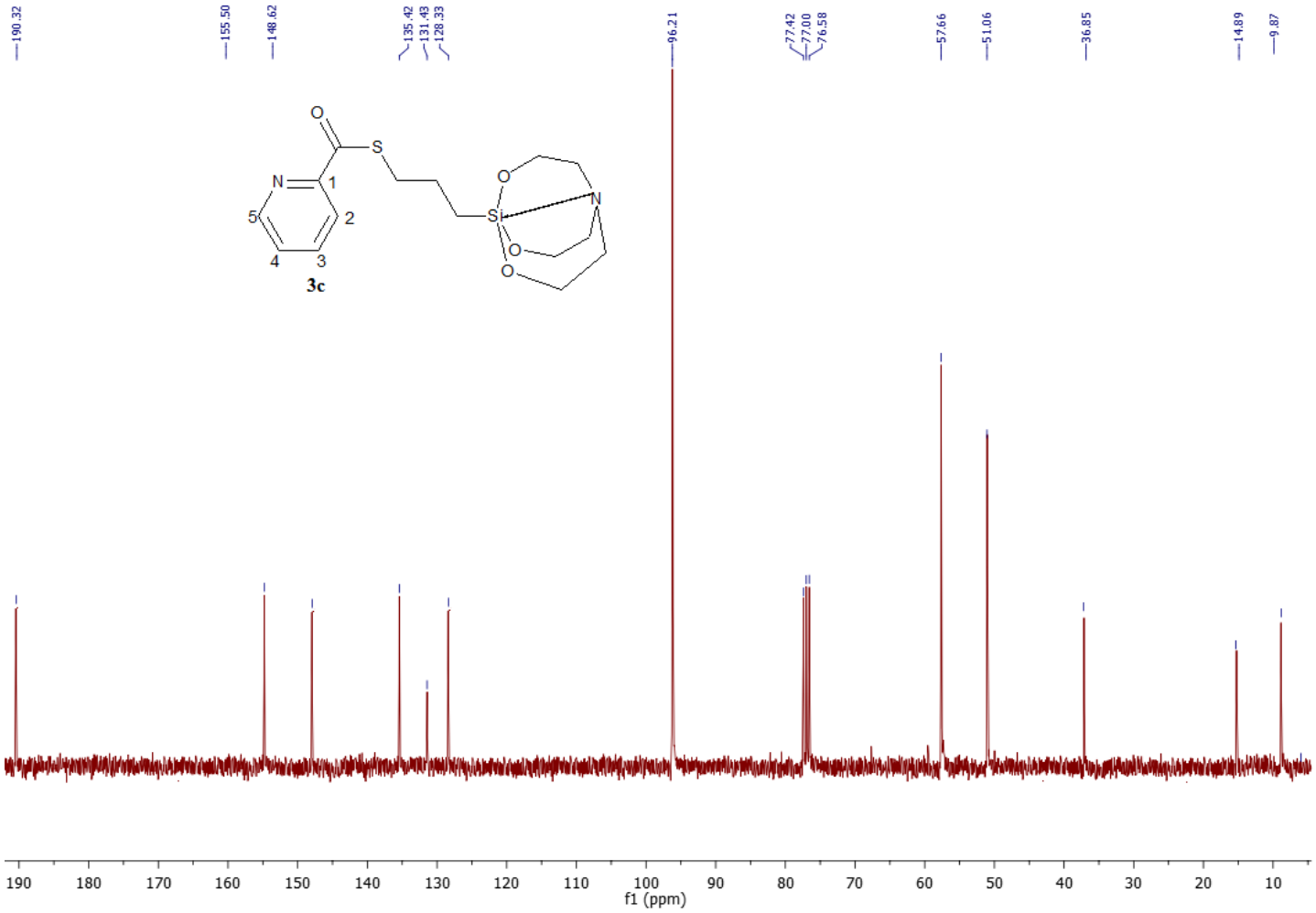

Fig. S36 ^{13}C NMR spectrum of **3c**

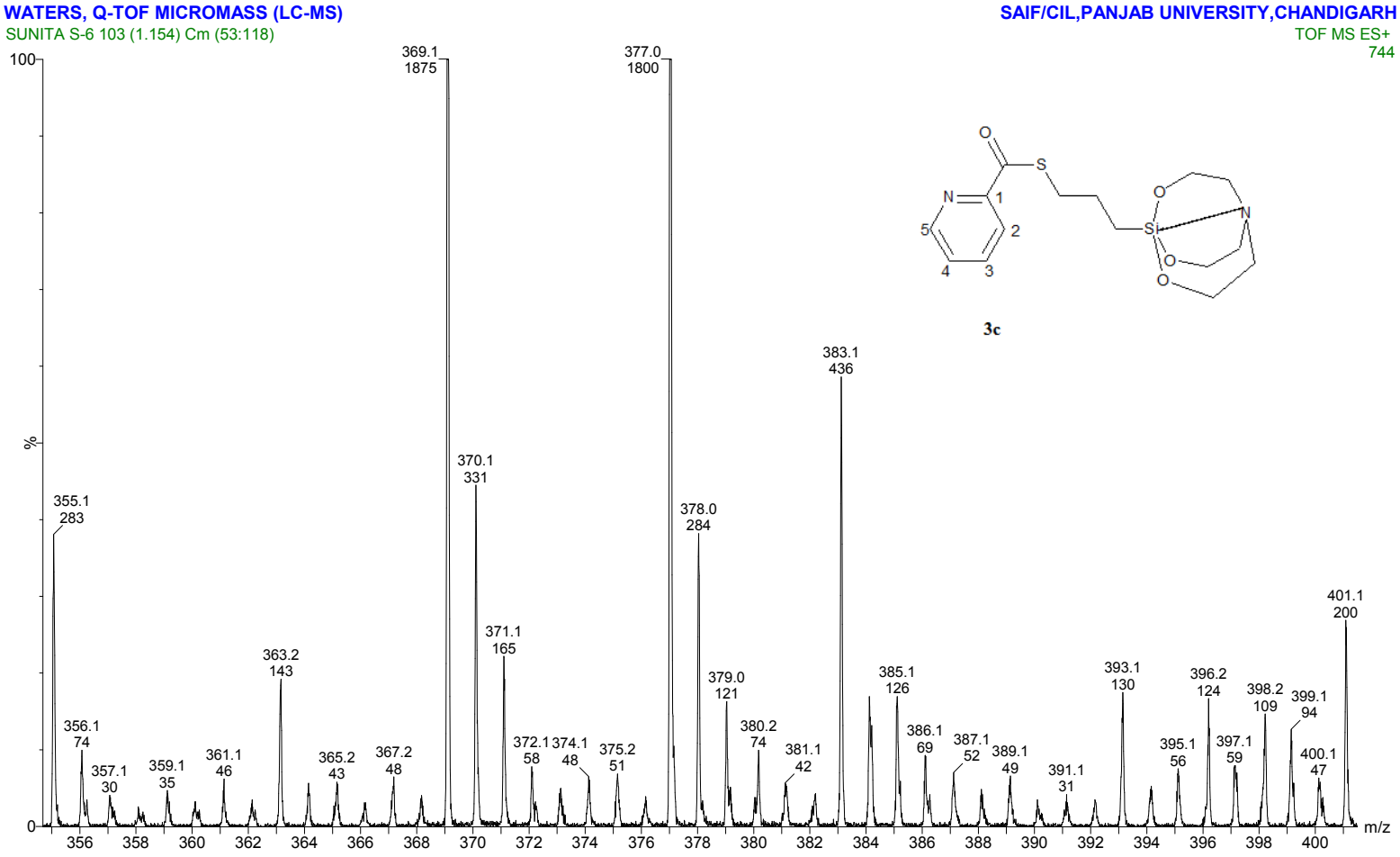

Fig. S37 Mass spectrum of **3c**

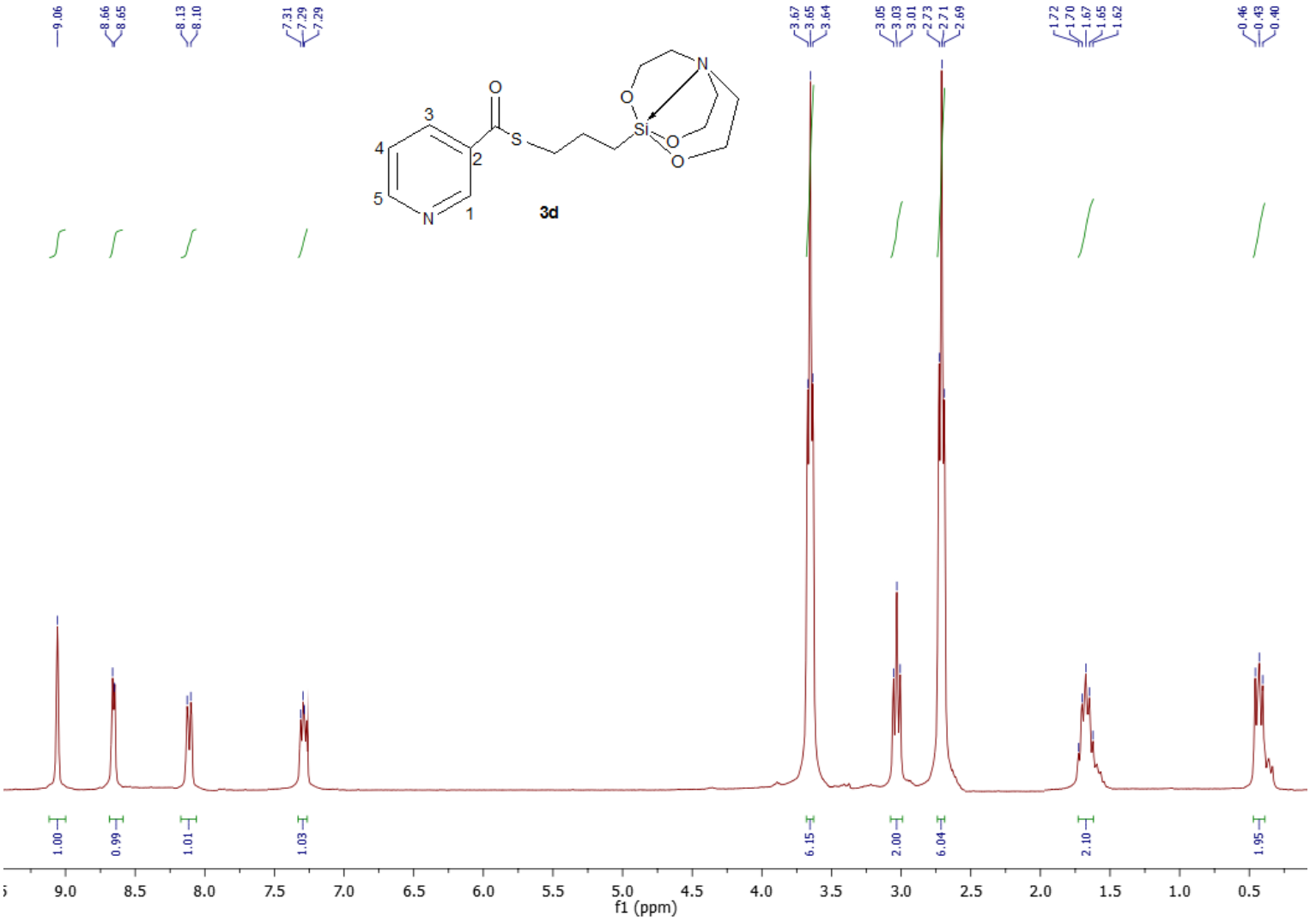

Fig. S38 ^{1}H NMR spectrum of **3d**

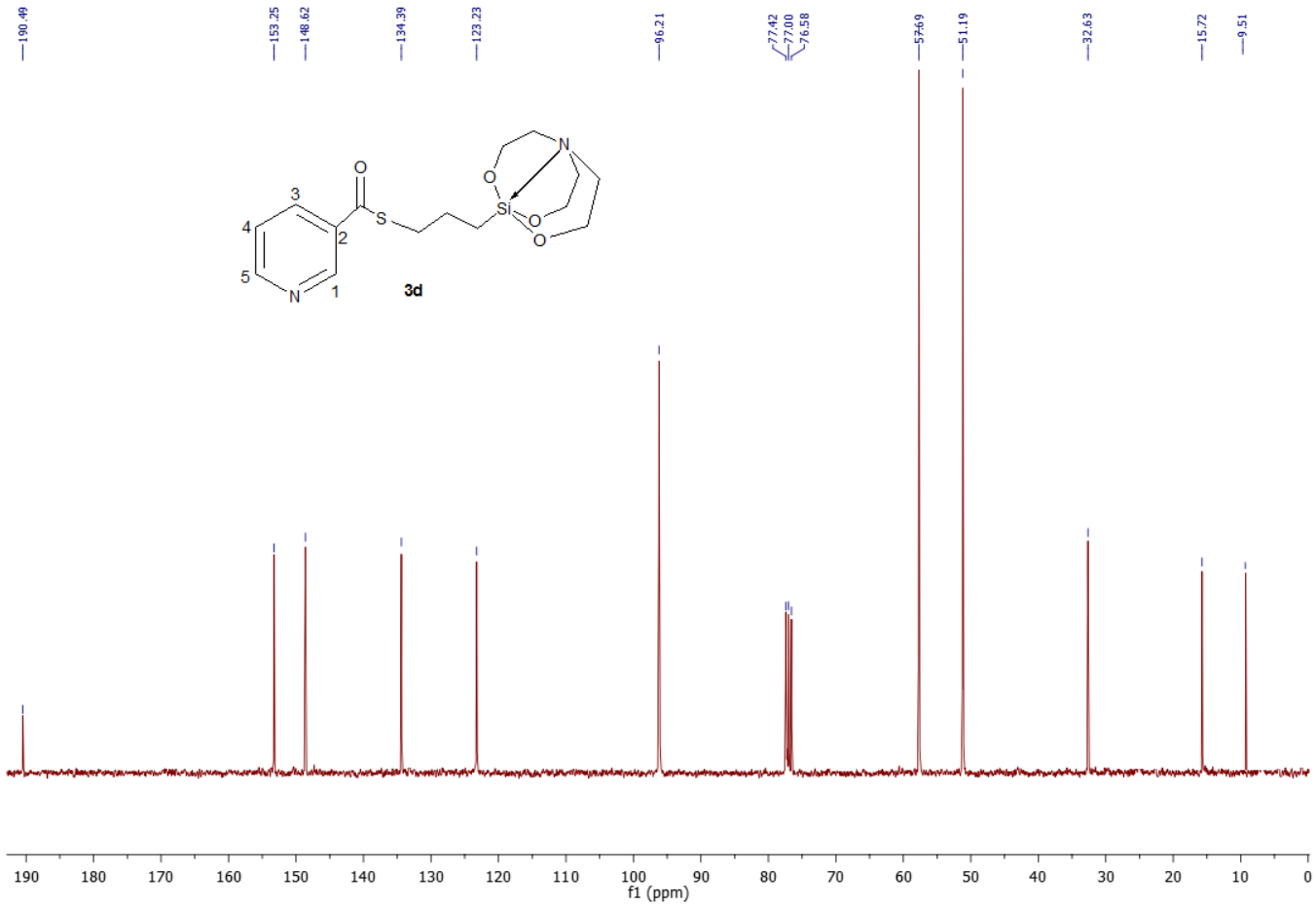

Fig. S39 ^{1}H NMR spectrum of **3d**

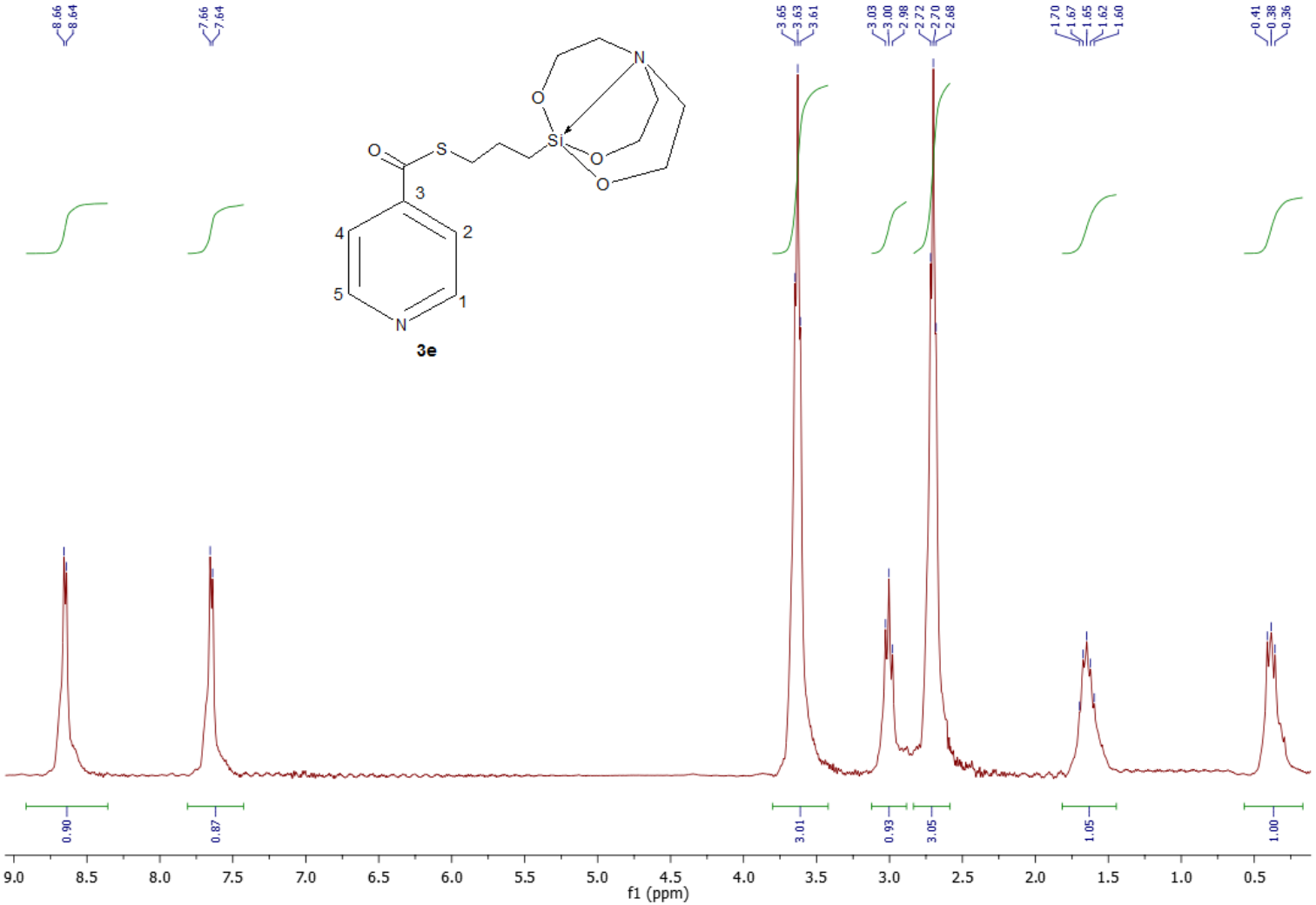

Fig. S40 ^{1}H NMR spectrum of **3e**

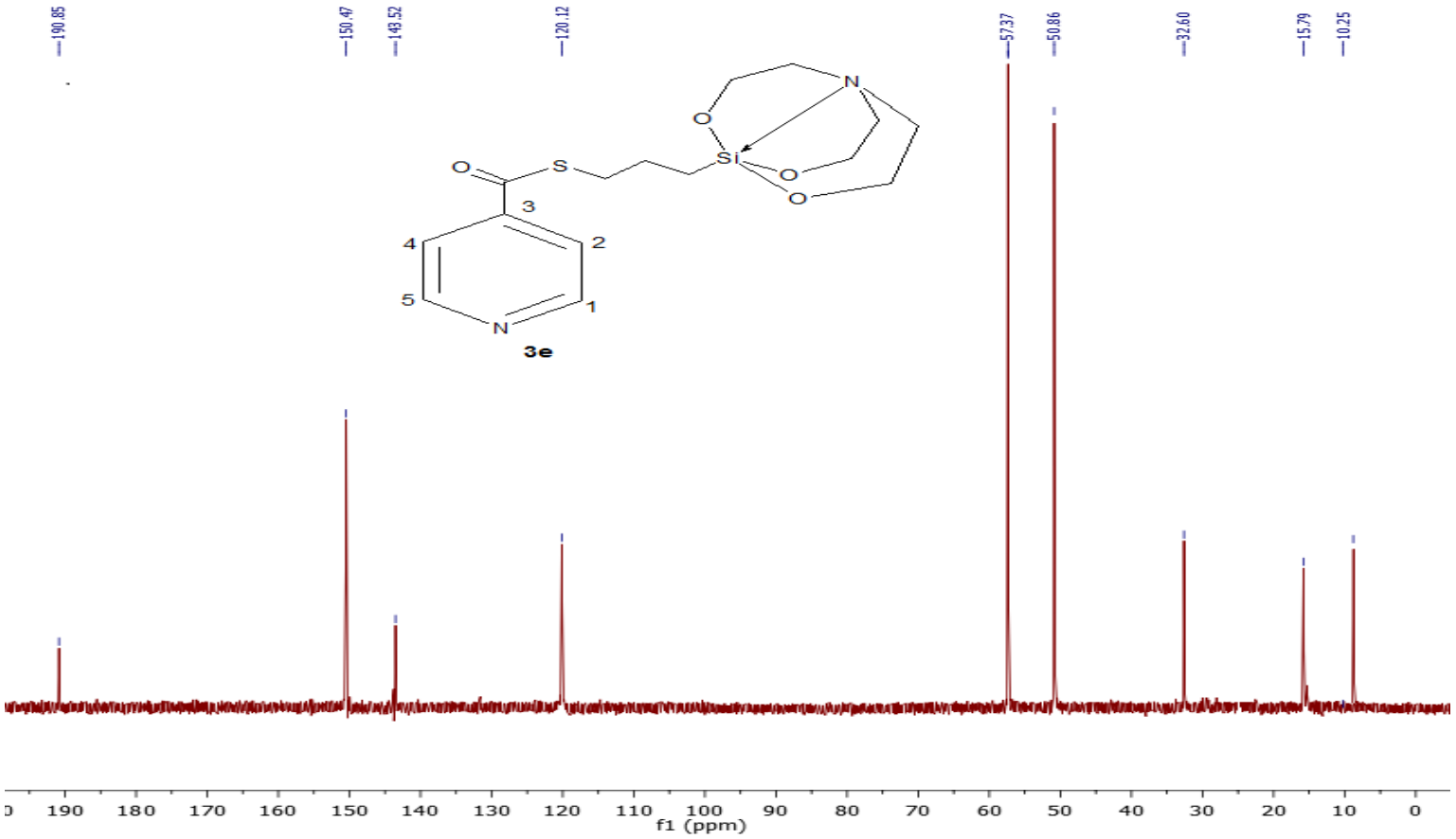

Fig. S41 ^{13}C NMR spectrum of **3e**

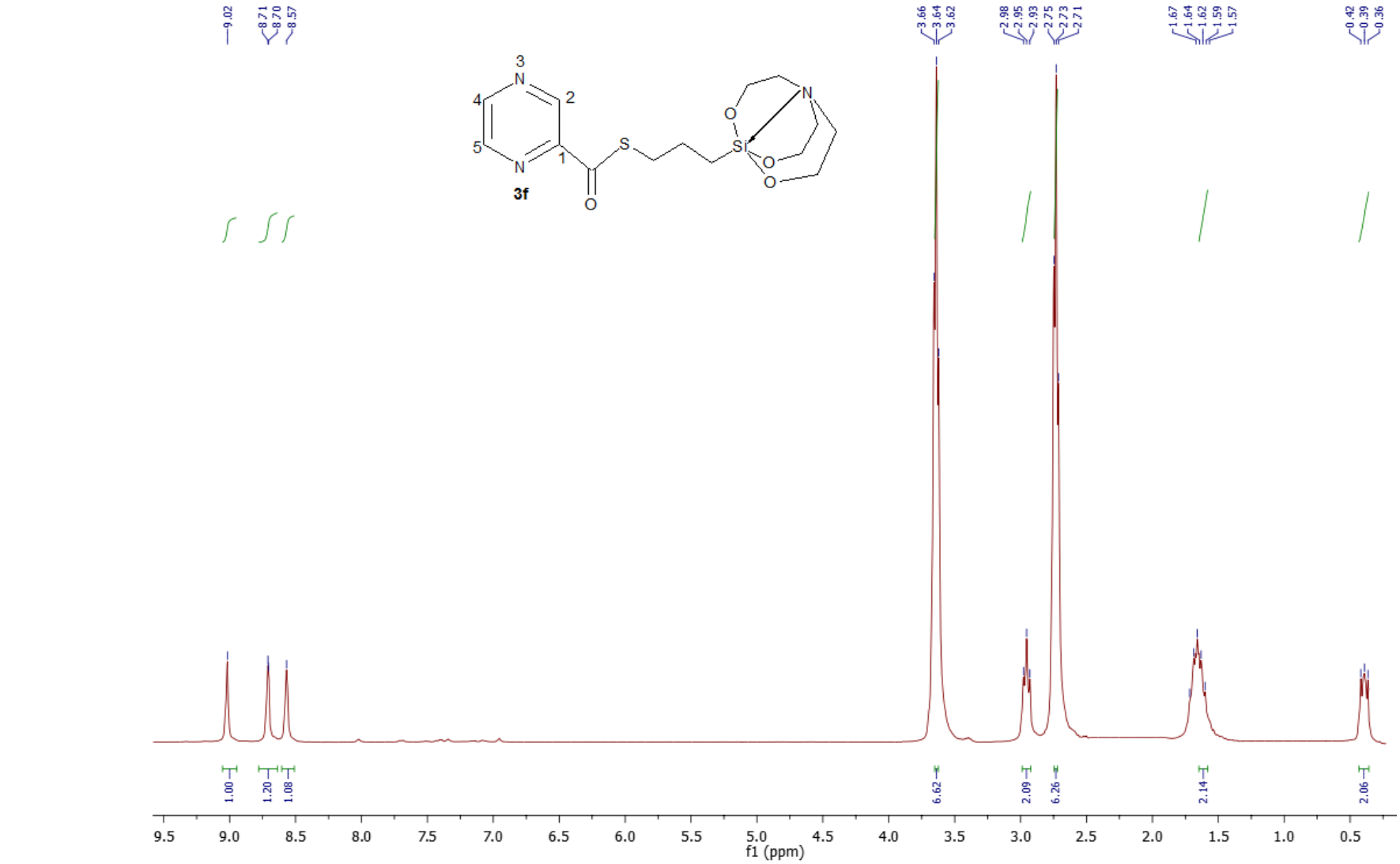

Fig. S42 ^{1}H NMR spectrum of **3f**

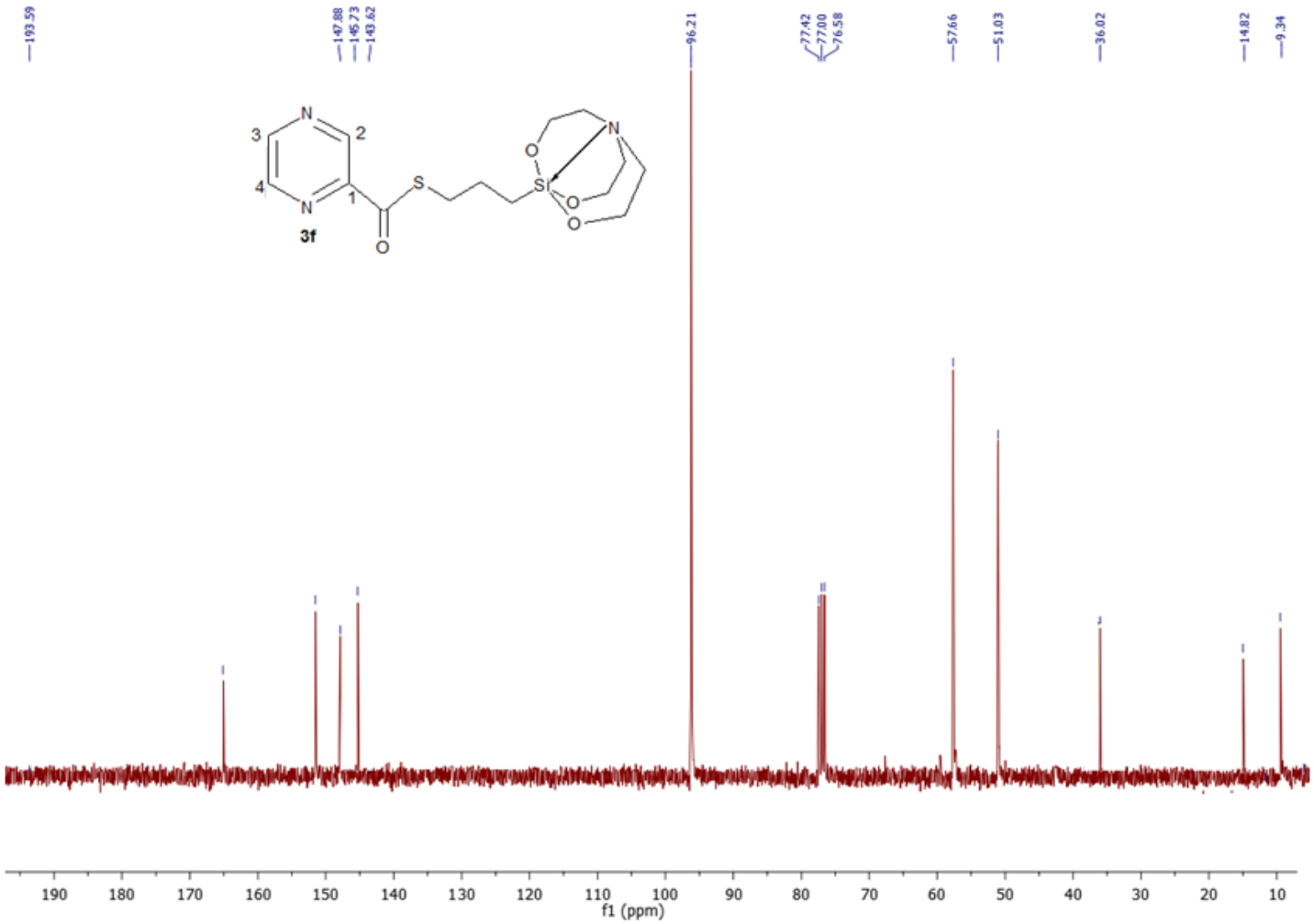

Fig. S43 ^{13}C NMR spectrum of **3f**

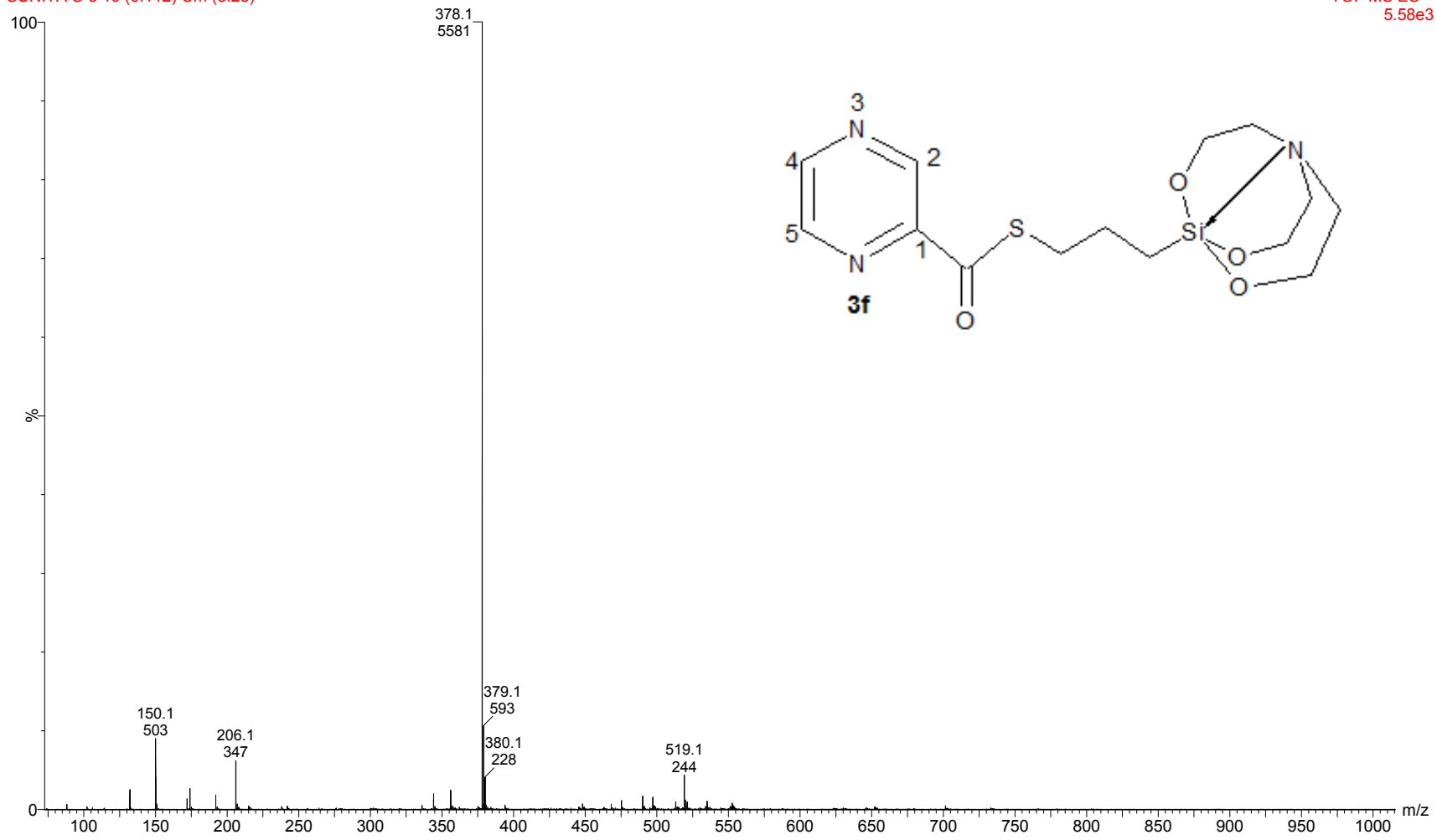

Fig. S44 Mass spectrum of **3f**

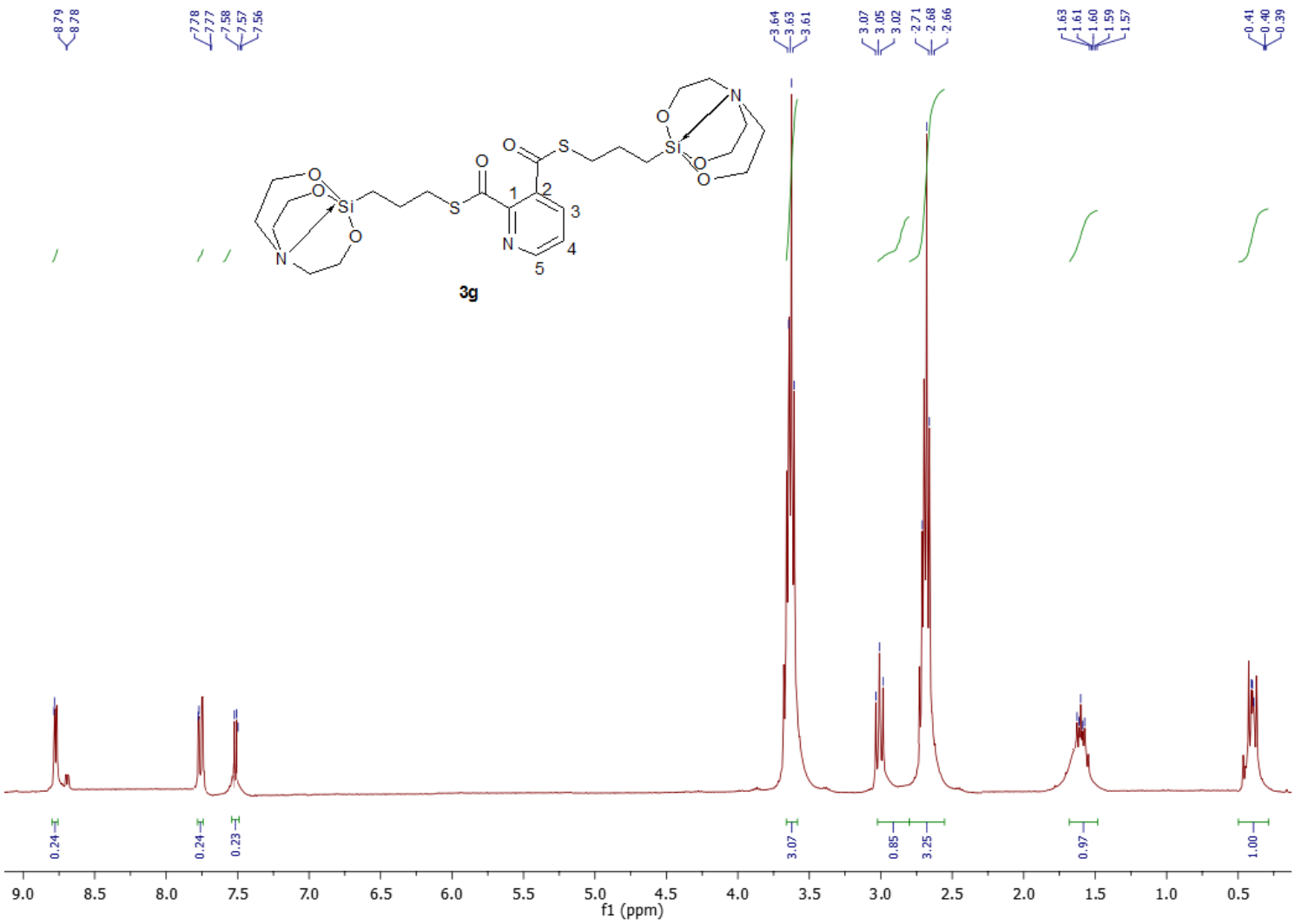

Fig. S45 ^{1}H NMR spectrum of **3g**

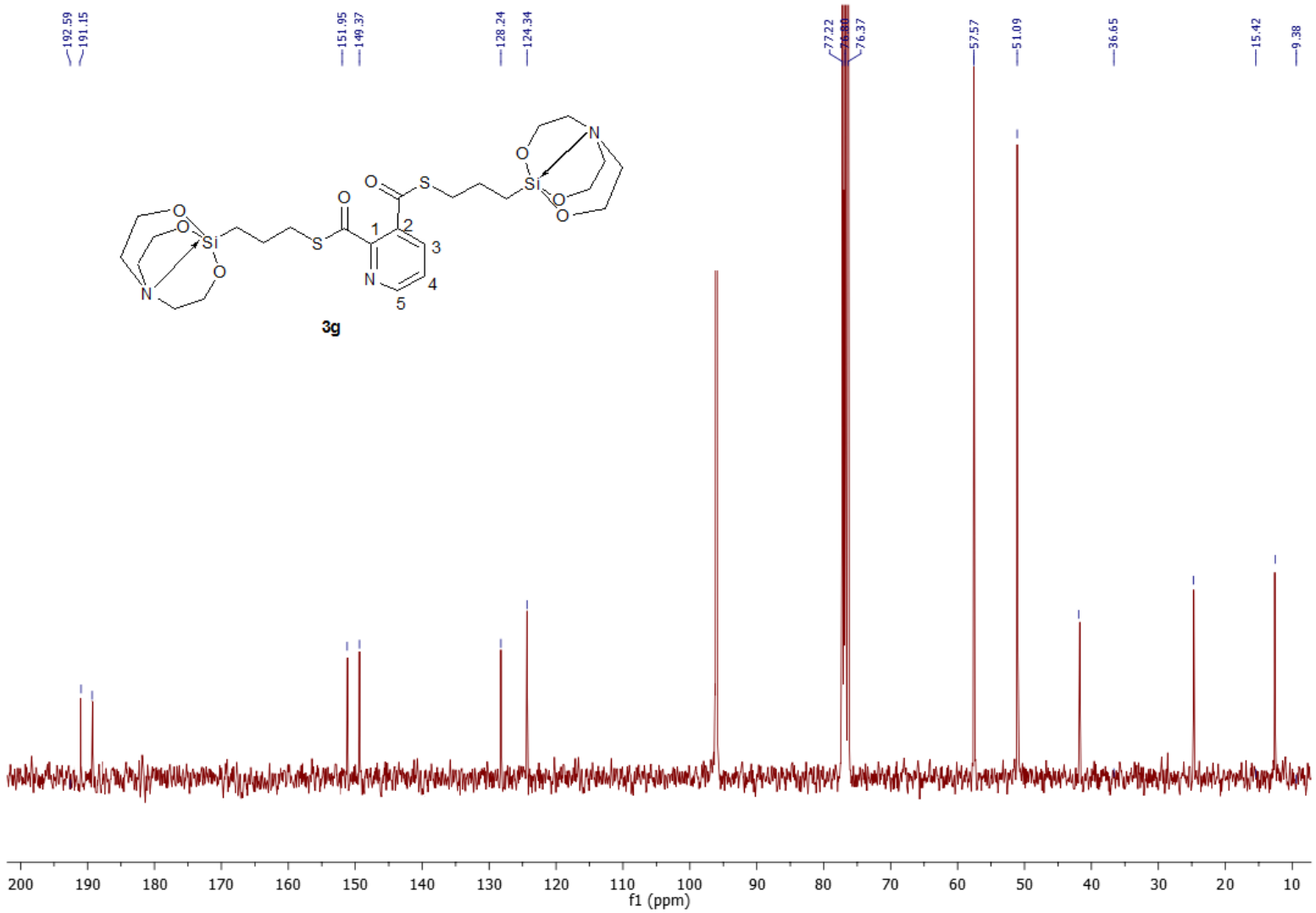

Fig. S46 ^{13}C NMR spectrum of **3g**

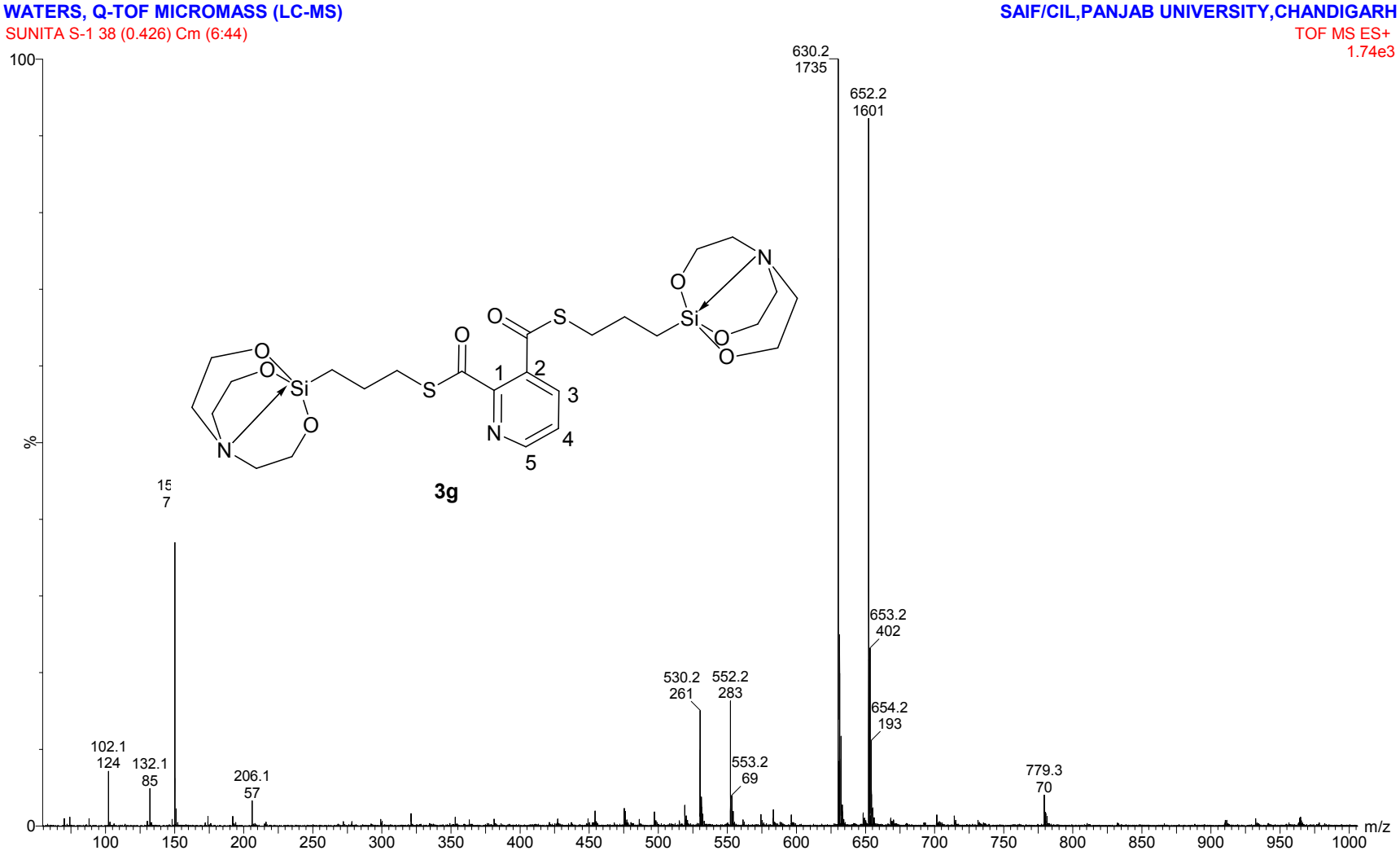

Fig. S47 Mass spectrum of **3g**

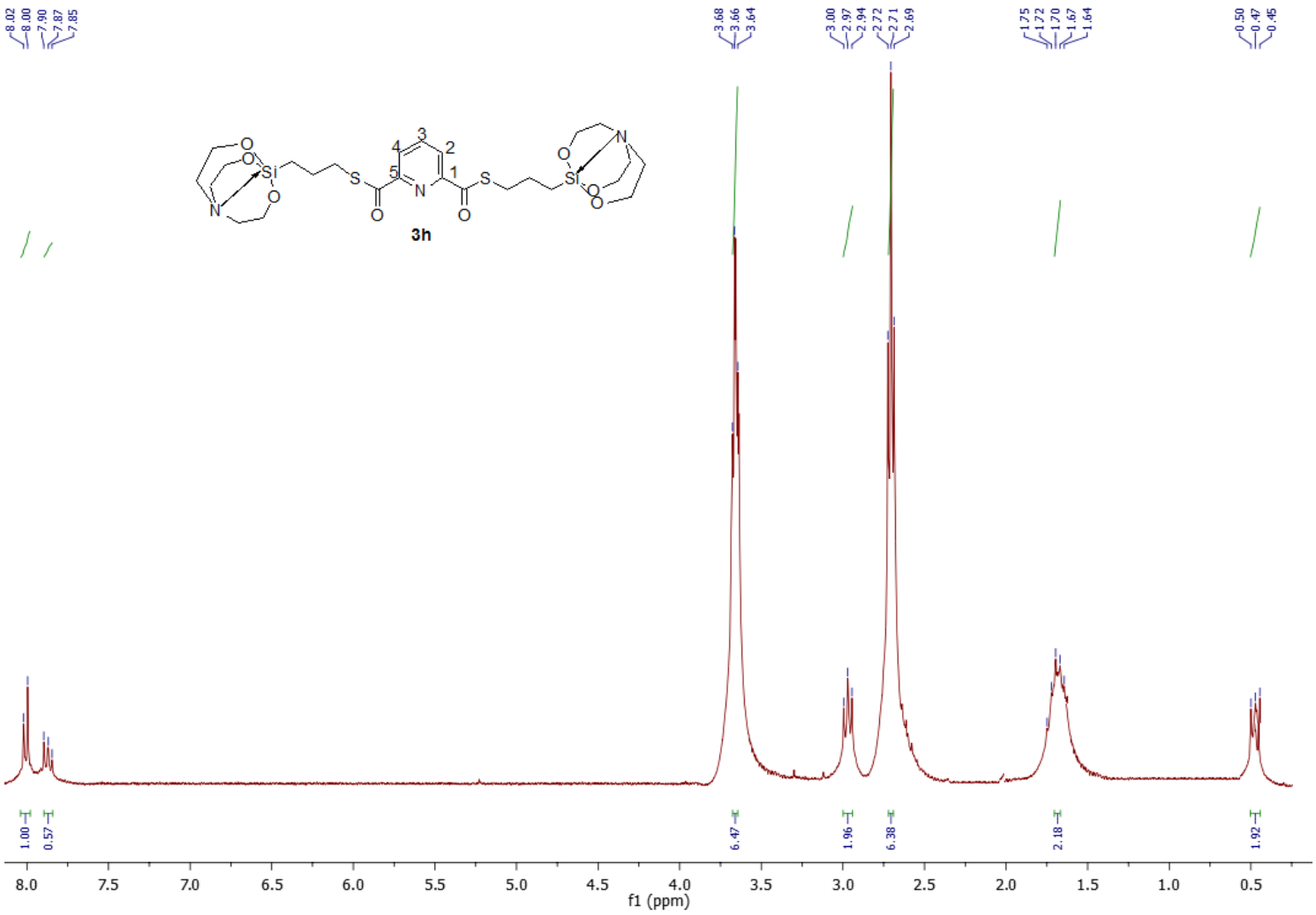

Fig. S48 ^{1}H NMR spectrum of **3h**

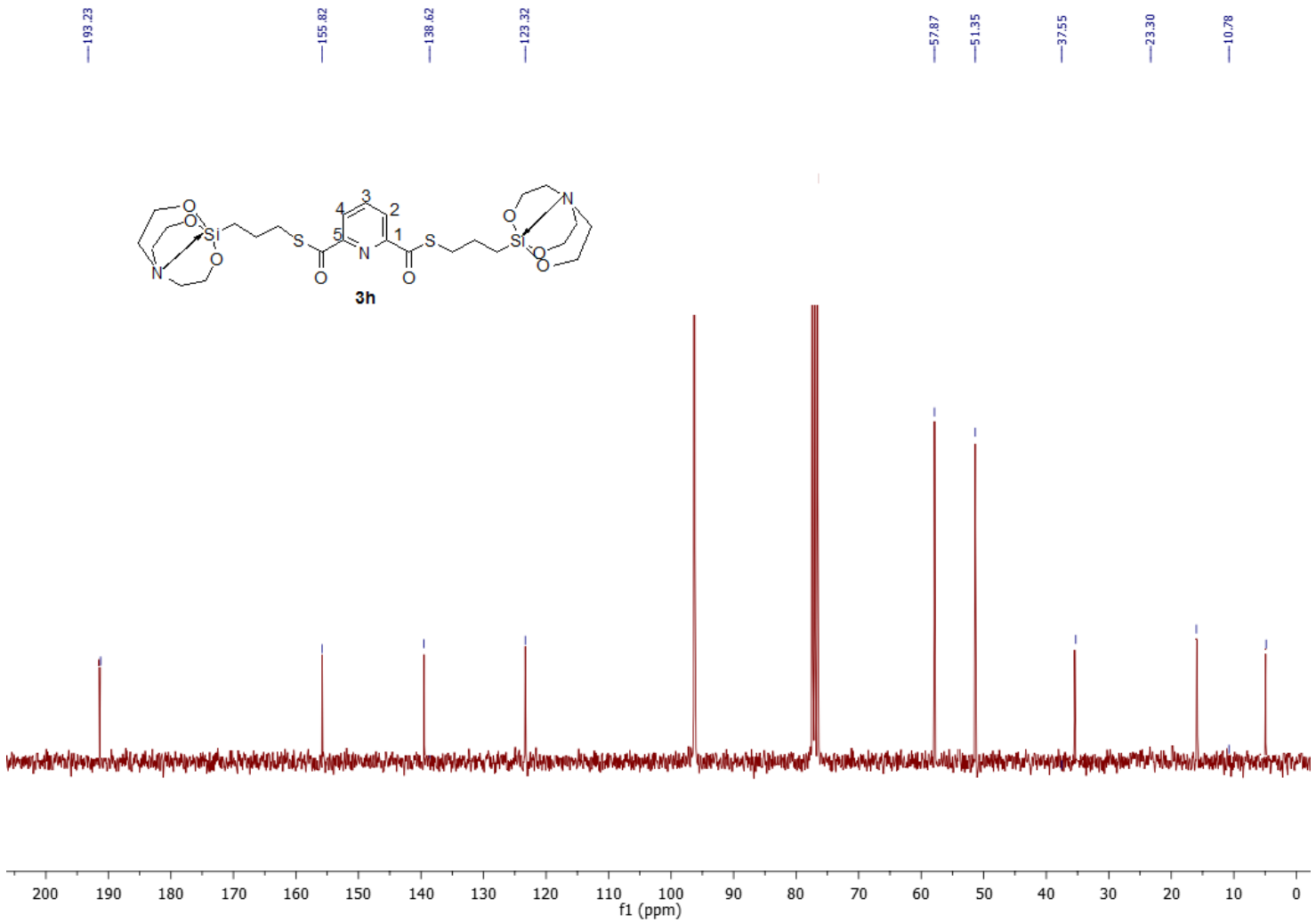

Fig. S49 ^{13}C NMR spectrum of **3h**